J. theor. Biol. (1998) **195,** 481–504
Article No. jt980808

Mathematical Models for Motile Bacterial Transport in Cylindrical Tubes*

KEVIN C. CHEN†‡, ROSEANNE M. FORD†ζ AND PETER T. CUMMINGS§

† *Department of Chemical Engineering, University of Virginia, Charlottesville, VA* 22903-2442, *U.S.A.*, § *Department of Chemical Engineering, University of Tennessee, Knoxville, TN* 37996-2200, *U.S.A. and Chemical Technology Division, Oak Ridge National Laboratory, Oak Ridge, TN* 37831-6268, *U.S.A.*

(*Received on* 9 *December* 1997, *Accepted in revised form* 28 *July* 1998)

Mathematical models considering motile bacterial transport within a geometrically restrictive cylindrical tube were developed. Two macroscopic transport parameters, the random motility coefficient as a self-diffusion coefficient of the cell population and the chemotactic velocity as a chemical-induced velocity, were derived. The three-dimensional cell balance equation was reduced to forms similar to Segel's one-dimensional phenomenological cell balance equations with additional modifications for bacteria–wall interactions. Two conceptually different approaches accounting for such interactions were presented. The first approach parallels treatments in the gas kinetic theory by viewing bacterial interactions with walls as collisions and subsequent diffusive/specular reflections, which led to the Bosanquet formula for the bacterial diffusion coefficient. Based on the experimental observation that bacterial swimming motion is guided by a straight tube, the second approach considered modifications in the bacterial swimming orientation as a consequence of various long-range interactions with the tube surface. A phenomenological turning model capable of aligning bacterial motion along a tube axis was proposed. The model predicts that under the geometrical restriction of a small cylindrical tube, the macroscopic bacterial transport resulting from the proposed turning model can exhibit behavior that ranges from dimensionally reduced diffusion to pure wave propagation, depending on the influence of the tube diameter on the reversal probability in the bacterial swimming motion. Our theoretical model provides explicit equations that explain how such a transition can occur. The predicted results were then qualitatively compared with experimental data from the literature. As a preliminary comparison, we concluded that bacterial transport in cylindrical tubes of diameter 10 μm remains in the mode of dimensionally reduced diffusion, and shifts to a wave motion when the tube diameter decreases to 6 μm.

1. Introduction

Self-propelled by rotating flagella, peritrichous bacteria such as *Escherichia coli* and *Salmonella typhimurium* exhibit random-walk behavior while swimming in a bulk phase. Berg & Brown (1972) observed that *E. coli* bacteria swim along

* Part of this work has been presented at the AIChE annual meeting, Chicago, IL, 11–17 November 1996.

ζ Author to whom correspondence should be addressed.
‡ Present address: Department of Physiology and Neuroscience, NYU Medical Center, 550 First Avenue, New York, NY 10016, U.S.A.

0022–5193/98/024481 + 24 $30.00/0

in approximately straight paths intermittently interrupted by a tumble due to a sudden reversal of the flagellar rotation. After a tumble, the swimming mode is resumed and the next swimming direction is randomly oriented. The self-propelled, irregular locomotion exhibited by motile bacteria resembles the random walk of gaseous molecules in Brownian diffusion. Hence at a population level, bacterial motility has long been quantified by the so-called random motility coefficient μ^o which in nature is similar to the molecular self-diffusion coefficient. A well-accepted expression based on persistent random walks (Lovely & Dahlquist, 1975) is

$$\mu^o = \frac{v^2}{3p_1(1-\psi)} \tag{1}$$

with v being the bacterial mean swimming speed (μm s^{-1}) in three dimensions, p_1 the isotropic tumbling frequency (s^{-1}) in the absence of spatial chemical gradients, and ψ the index of directional persistence (Othmer *et al*., 1988), explicitly defined as the mean cosine of the turn angle between two successive swimming directions.

Bacteria can sense changes in their environment via thousands of protein receptors rooted in their cytoplasmic membranes. These receptors, like enzymes, can be bound by specific chemical molecules to which they are exposed. It has been verified that bacteria change their tumbling frequencies by mediating the flagellar motors via a temporal comparison of receptor occupancy (Macnab & Koshland, 1972; Segall *et al*., 1986; Spudich & Koshland, 1975). Thus in the presence of a spatial attractant gradient, the bacterial tumbling frequency decreases as they swim spatially upwards toward the attractant source. Such an anisotropic tumbling frequency induced by the spatial chemical gradients and their motility can result in directed migrations of the whole population, a phenomenon termed chemotaxis. Experiments demonstrating traveling bands of a bacterial population resulting from chemotaxis can be found in Adler (1966), Ford *et al*. (1991), Holz & Chen (1979), and Wang & Chen (1986).

1.1. GAS KINETIC THEORY

By analogy to Brownian diffusion in the bulk, the diffusive transport of motile bacteria within a geometrically restrictive phase is likely described and quantified through the concept of gaseous Knudsen diffusion in which molecule–wall collisions are as important as molecule–molecule collisions (Barton & Ford, 1995; Duffy *et al*., 1995). If μ_d is equivalent to the self-diffusion coefficient of bacteria within a long cylindrical tube of diameter d equal to the average pore size of a porous medium, given that resistance to transport is a *linear* sum of the resistance of both molecule–molecule collisions and molecule–wall collisions, the Bosanquet formula (Pollard & Present, 1948)

$$\frac{1}{\mu_d} = \frac{1}{\mu^o} + \frac{1}{\mu^k} \tag{2}$$

was employed to estimate the diffusion coefficient μ_d in a tube. In eqn (2) μ^k is known as the Knudsen diffusivity (Knudsen, 1909). Its most general form is given by

$$\mu^k = \frac{vd}{3}\left(\frac{2-f}{f}\right) \tag{3}$$

with f being the sticking coefficient, or the fraction of impinging molecules leaving the solid surface in the mode of diffusive reflection after instantaneous sticking on the solid surface (Derjaguin & Fedyakin, 1993). In practice f is taken to be 1 (purely diffusive reflection) for gas molecules.

Assuming $f = 1$ and inserting both eqns (1) and (3) into eqn (2) yields a new expression for μ_d,

$$\mu_d = \frac{v^2}{3p_1(1-\psi)}\left[\frac{1}{1+\mathrm{Kn}/(1-\psi)}\right] \tag{4}$$

with the Knudsen number Kn ($=\lambda/d$) defined to be the ratio of the bacterial mean run length λ to the tube diameter d. Equation (4) has been used to analyse the experimental measurements of bacterial penetration profiles in sand columns (Barton & Ford, 1995). Nevertheless, application of eqn (2) to bacterial transport does not provide a complete analysis because chemotaxis in the same cylindrical tube—an essential part in studying the transport of chemotactic bacteria—remains unspecified. Recently Barton & Ford (1997) modified Segel's one-dimensional phenomenological model (Segel, 1977) to relate the

effect of pore structures by incorporating specific collision terms in the overall reversal probabilities to the bacterial transport equations in porous media. To our knowledge, there exists no other fundamental theory to date which relates chemotaxis with pore size based on first principles of physics. Because a study of bacterial transport in a long cylindrical tube of diameter comparable to the average pore size may reveal insights for applications in porous media, one goal of this work is to provide such a theoretical basis for quantifying the chemotactic velocity within a narrow tube. We will show later that the Bosanquet formula for the bacterial random motility coefficient can be derived from a three-dimensional cell balance equation (Alt, 1980; Ford & Cummings, 1992) upon invoking necessary assumptions consistent with gas kinetic theory. Following the derivation leading to eqn (2), the corresponding chemotactic velocity resulting from the same analysis is thereby determined.

Nevertheless, the dependence of μ_d on the tube diameter as predicted by eqn (4) is not consistent with what has been observed experimentally. The capillary array experiment of Berg & Turner (1990) was a pioneering effort in quantifying bacterial transport rates in long cylindrical tubes. They found that in the absence of an attractant gradient, the bacterial diffusion coefficient in 10 μm-diameter tubes was even larger than in 50 μm-diameter tubes. This peculiar phenomenon was attributed to the alignment of bacterial running segments with the axes of the smaller tubes, thus resulting in a predominantly one-dimensional random motion. As a complement to Berg & Turner's macroscopic experiment, the microscopic single-capillary experiment conducted by Liu & Papadopoulos (1995, 1996, 1997) visualized single-cell movement in a fine capillary. In addition to verifying the alignment behavior, they also reported a valid Poisson process for the tumbling frequency and an unreduced mean swimming speed for *E. coli* K-12 within the capillary.

The failure of eqn (4) to agree in its trend with experiments is because the validity of applying eqn (4) to bacterial self-diffusion in small pores requires several assumptions, most of which are violated. Frymier *et al*. (1995) and Liu & Papadopoulos (1995) observed that the interaction between a cell and the wall surface is rarely a collision. When bacteria swam toward a solid wall, the straight trajectories were smoothly deflected and the bacteria began swimming *along* the surface before the next tumbling event (Frymier *et al*., 1995; Frymier & Ford, 1997). This deflection from its straight swimming trajectories can be attributed to the large hydrodynamic resistance for a rigid sphere approaching an impenetrable wall through a stagnant fluid (Happel & Brenner, 1983). The hydrodynamic solution of Ramia *et al*. (1993) also produced the same phenomenon. Furthermore, successful derivations of eqns (2) to (4) rest upon neglecting any long-range interactions so that the cell number density in velocity space is uniformly distributed. Since bacteria in small capillaries show predominantly one-dimensional motion, it implies that the cell angular probability density distribution is elongated towards both ends of the tube axis. Although the swimming segments can still undergo off-line motion, the randomness is greatly reduced in the other two dimensions perpendicular to the tube axis.

1.2. HINDERED DIFFUSION THEORY

We also found the hindered diffusion theory (Anderson & Quinn, 1974; Anderson, 1981; Brenner & Gaydos, 1977; Deen, 1987) unsuitable for the study of motile bacterial transport within a small tube. In essence, the hindered transport theory predicts a rapidly decreasing diffusion coefficient in the *configurational regime* (a regime in which the tube diameter and the particle proximal size, instead of the mean run length, are the two dominant length scales (Froment & Bischoff, 1979) due to the steric restriction of the solute's excluded volume and the enhanced solvent drag. This prediction contradicts the observation reported in Berg & Turner's experiment. Besides, motile bacteria move about mainly by self-propulsion, not by Brownian motion which is easily retarded by fluid drag, whereas the mean swimming speed was observed to be unaffected in small pores (Liu & Papadopoulos, 1996; Biondi & Quinn, 1998; Phillips, 1992) irrespective of the enhanced hydrodynamic resistance.

1.3. MOTIVATION

Due to the fact that present studies still remain at the empirical level and that existing models borrowed either from gas kinetic theory or from hindered diffusion theory cannot successfully resolve the underlying discrepancies, another goal in this work is to establish a phenomenological mathematical model that will set a precedent for the whole assessment of bacterial transport phenomena in long cylindrical tubes. The model is phenomenological in the sense that it does not provide insights into the true mechanism behind the exhibited behaviors, but rather qualitatively captures the key features as exhibited in numerous experimental observations. The conceptual basis for this model is the modification of the global turning probability density distribution based on the observed bacterial transport rates and swimming behaviors illustrated in two representative experiments (Berg & Turner, 1990; Liu & Papadopoulos, 1995, 1996, 1997). This approach of studying bacterial swimming orientation, combined with conceptual modeling, helps provide a more structured understanding of the bacterial transport mechanism in geometrically restrictive cylindrical tubes.

An outline of this work follows. In Section 2 we present the three-dimensional cell balance equation symmetrically reduced in a cylindrical geometry along with the relevant assumptions. In Section 3 two macroscopic transport parameters, the random motility coefficient and the chemotactic drift velocity, are derived using the traditional gas kinetic model. The theoretical results, although in disagreement with experimental observations, can help us examine the underlying assumptions that require further modifications. Due to the inability of the transport parameters derived from the gas kinetic model to predict the observed trends in confined geometry, we proposed an orientation model in Section 4 that modifies the phenomenological interactions between the bacterial turning probability density distribution and the pore diameter. In Section 5 we compare the model predictions with experimental data from the literature and discuss the possible guidance impact on bacterial random walks in porous media via computer simulations. In Section 6 we summarize our conclusions.

2. Symmetrical Reduction of the Cell Balance Equation

The bacterial number density, $n(\mathbf{t}, \hat{\mathbf{s}}, t)$, in an aqueous phase is assumed to be a function of the position $\mathbf{r}$, the swimming velocity $\mathbf{v}(=v\hat{\mathbf{s}})$, and the time t. In our study v is assumed to be a *constant* swimming speed. The quantity $n(\mathbf{r}, \hat{\mathbf{s}}, t)\, d\mathbf{r}\, d\hat{\mathbf{s}}$ represents the expected bacterial number at time t in the spatial volume element $d\mathbf{r}$ about the position $\mathbf{r}$, traveling in the swimming direction which lies in the solid angle $d\hat{\mathbf{s}}$ about $\hat{\mathbf{s}}$. To formulate a cellular balance equation regarding the number density $n(\mathbf{r}, \hat{\mathbf{s}}, t)$, we further introduce the definitions of the following field functions:

- $p_t(\mathbf{r}, \hat{\mathbf{s}}\cdot\nabla a, t)$ = the probability frequency (probability per unit time) that a bacterium at position $\mathbf{r}$ swimming in direction $\hat{\mathbf{s}}$ subject to a spatial chemical gradient ∇a will tumble. The tumbling frequency p_t as a field function indirectly arises from a mechanism that compares the temporal change in the number of chemotactic receptors bound with attractant molecules. This mechanism, according to the mass action law of Weber (Mesibov *et al*., 1973), depends solely on the dot product between the swimming vector and the spatial chemical gradient, $\hat{\mathbf{s}}\cdot\nabla a(\mathbf{r}, t)$. Note that the variables $\mathbf{r}$ and t in p_t are taken to be explicit here.
- $\kappa(\mathbf{r}, \hat{\mathbf{s}}'|\hat{\mathbf{s}})$ = the turning probability density function that a bacterium at $\mathbf{r}$, given the previous swimming direction $\hat{\mathbf{s}}'$, tumbles and turns with the probability $\kappa(\mathbf{r}, \hat{\mathbf{s}}'|\hat{\mathbf{s}})\, d\hat{\mathbf{s}}$ into $d\hat{\mathbf{s}}$ about the new direction $\hat{\mathbf{s}}$. In an unbounded fluid, $\kappa(\hat{\mathbf{s}}'|\hat{\mathbf{s}})$ is assumed to be a function of $\hat{\mathbf{s}}'\cdot\hat{\mathbf{s}}$ only.

With these notations, the cell balance equation can be written as (Alt, 1980; Ford & Cummings, 1992)

$$\begin{aligned}\frac{\partial n(\mathbf{r}, \hat{\mathbf{s}}, t)}{\partial t} = & -v\hat{\mathbf{s}}\cdot\nabla n(\mathbf{r}, \hat{\mathbf{s}}, t) \\ & - p_t(\mathbf{r}, \hat{\mathbf{s}}\cdot\nabla a, t) n(\mathbf{r}, \hat{\mathbf{s}}, t) \\ & + \int p_t(\mathbf{r}, \hat{\mathbf{s}}'\cdot\nabla a, t) n(\mathbf{r}, \hat{\mathbf{s}}', t) \\ & \times \kappa(\mathbf{r}, \hat{\mathbf{s}}'|\hat{\mathbf{s}})\, d\hat{\mathbf{s}}'. \end{aligned} \tag{5}$$

In eqn (5) the first term on the right-hand side accounts for the convective contribution of smoothly swimming bacteria in the direction $\hat{\mathbf{s}}$ passing through the point $\mathbf{r}$ without tumbling. For those bacteria that do tumble at $\mathbf{r}$, they are taken into account by the second and third terms, representing such contributions of bacterial tumbling out of and into the specific direction $\hat{\mathbf{s}}$ at $\mathbf{r}$, respectively. Equation (5) is a *linear* integro-differential equation for motile bacterial transport adopted from a simplified Boltzmann theory. The linearity comes from the implicit assumption that the change of swimming directions is only caused by bacterial automatic tumbles and subsequent turnings. This assumption is usually valid due to the low number density in bacterial suspensions ($10^6 \sim 10^9$ cells ml^{-1}, which gives the cell volume density around $10^{-6} \sim 10^{-3}\,\mathrm{cm}^3\,\mathrm{ml}^{-1}$, assuming a size of a bacterium is $1 \times 2\ \mu\mathrm{m}$). Because of this dilute number density, intercellular forces can be neglected and each bacterium in a bulk suspension behaves as if were alone. Otherwise, one would expect to see additional *nonlinear* terms in eqn (5) accounting for bacterial mutual interactions.

With a small capillary having a diameter comparable to the length of bacterial flagella, it is assumed that only one bacterium is present in the tube at a time. Thus we still need not consider intercellular interactions but the cell–wall interactions become paramount. Under this circumstance, the statistical concept (Brenner & Gaydos, 1977) is employed by assuming a large number of identical, parallel capillaries and taking $n(\mathbf{r}, \hat{\mathbf{s}}, t)$ as the ensemble average of all capillaries at a given location and instant in time. As long as the ensemble is large enough, the ensemble-averaged probability density can represent the continuous cell number density distribution. Without further explanation, this continuum description will be adopted throughout this study.

Due to the inherent complexities in eqn (5), closed-form solutions are difficult to find except for very simple and highly idealized situations. In some symmetrical geometries (e.g. plane, spherical, and cylindrical geometries), eqn (5) simplifies considerably. In the following context we limit our attention to a cylindrical geometry. Let η be the coordinate perpendicular to the axis of symmetry (taken to be the z-axis) and φ the azimuthal angle around z [see Fig. 1(a)]. The position vector $\mathbf{r}$ can be represented by the set of cylindrical coordinates (η, φ, z). However, the unit directional vector $\hat{\mathbf{s}}$ in velocity space is expressed in Cartesian coordinates in terms of spherical variables, $\hat{\mathbf{s}} = \sin\theta\cos\phi\hat{\mathbf{e}}_x + \sin\theta\sin\phi\hat{\mathbf{e}}_y + \cos\theta\hat{\mathbf{e}}_z$, in which $\hat{\mathbf{e}}_x$, $\hat{\mathbf{e}}_y$, and $\hat{\mathbf{e}}_z$ are the unit vectors representing the principal axes of x, y, and z, respectively. Both the azimuthal angles φ and ϕ are defined relative to $\hat{\mathbf{e}}_z$ with the reference set at $\hat{\mathbf{e}}_x$ as shown in Fig. 1(a). In the cylindrical geometry, the spatial chemical gradient is assumed to be one-dimensional and to be aligned with the z-axis. Then $\hat{\mathbf{s}}\cdot\nabla a = \cos\theta\nabla_z a$, leading to the simplified dependence of the tumbling frequency, $p_t(z, \theta, t)$. And $\kappa(\mathbf{r}, \hat{\mathbf{s}}'|\hat{\mathbf{s}})$ reduces to $\kappa(\eta, \hat{\mathbf{s}}'|\hat{\mathbf{s}})$ due to the assumption that

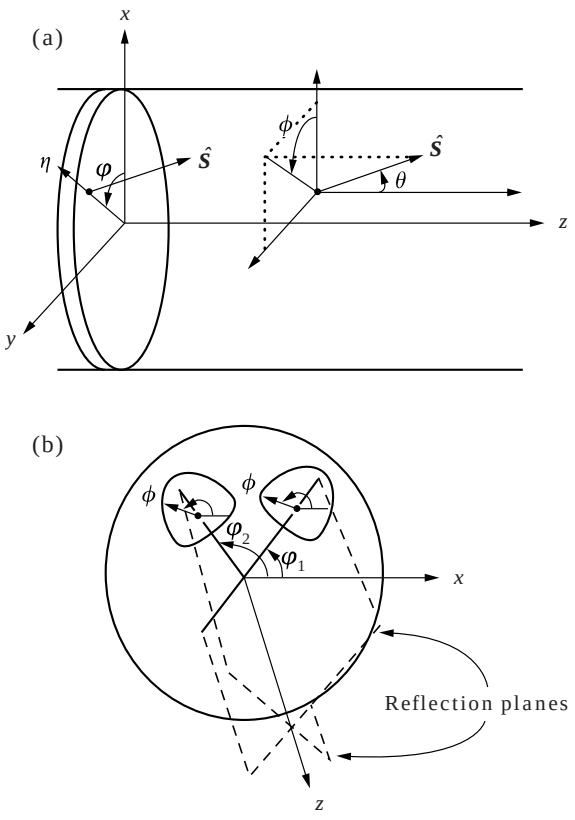

FIG. 1. (a) Cylindrical coordinates and the bacterial running direction expressed in spherical coordinates; (b) an imaginary bacterial angular number density distribution mapped onto the x–y plane to illustrate rotational symmetry.

the turning is independent of chemical gradients. Because

$$\frac{\partial}{\partial x} = \cos\varphi \frac{\partial}{\partial \eta} - \frac{\sin\varphi}{\eta}\frac{\partial}{\partial \varphi}$$

$$\frac{\partial}{\partial y} = \sin\varphi \frac{\partial}{\partial \eta} + \frac{\cos\varphi}{\eta}\frac{\partial}{\partial \varphi}$$

$$\frac{\partial}{\partial z} = \frac{\partial}{\partial z}$$

the convective term $\hat{\mathbf{s}}\cdot\nabla n$ becomes

$$\hat{\mathbf{s}}\cdot\nabla n = \sin\theta\cos(\phi-\varphi)\frac{\partial n}{\partial \eta} + \frac{\sin\theta}{\eta}\sin(\phi-\varphi)\frac{\partial n}{\partial \varphi} + \cos\theta\frac{\partial n}{\partial z}, \quad (6)$$

which means only the difference of φ and ϕ is involved as a single independent variable in the bacterial angular density distribution. Note that cylindrical geometry does not ensure $\partial n/\partial\varphi = 0$. Only the cell number density after being integrated over the azimuthal angle ϕ in velocity space will be independent of φ. Furthermore, symmetry in the cell density is introduced with respect to any plane containing the z-axis (the reflection plane). To facilitate understanding such a symmetry, we show in Fig. 1(b) two imaginary bacterial density distributions in velocity space mapped onto the x–y plane. Both mapped density distributions are on the circle of the same radial distance η, and only the azimuthal angles (φ_1 and φ_2) differ. The symmetry relative to the reflection plane further requires $|\phi-\varphi|$ as the sole variable. Thus, the cylindrical geometry applied to the bacterial density distributions leads to the rotational invariance,

$$n(\eta,\varphi,z,\theta,\phi,t) = n(\eta,z,\theta,|\phi-\varphi|,t). \quad (7)$$

That is, n is rotationally invariant if we simultaneously rotate φ and ϕ while keeping the absolute difference between them fixed.

If one integrates the bacterial number density over the cylindrical cross-section area by $\eta\,\mathrm{d}\eta\,\mathrm{d}\varphi$ and the azimuthal ϕ in velocity space by $\mathrm{d}\phi$, it follows that

$$\begin{aligned} N(z,\theta,t) &= \int_0^{2\pi}\int_0^{2\pi}\int_0^{d/2} n(\eta,z,\theta,|\phi-\varphi|,t)\eta\,\mathrm{d}\eta\,\mathrm{d}\varphi\,\mathrm{d}\phi \\ &= 2\pi\int_0^{2\pi}\int_0^{d/2} n(\eta,z,\theta,\phi,t)\eta\,\mathrm{d}\eta\,\mathrm{d}\phi \\ &= 2\pi\int_0^{2\pi}\int_0^{d/2} n(\eta,z,\theta,\varphi,t)\eta\mathrm{d}\eta\,\mathrm{d}\varphi \end{aligned} \quad (8)$$

where d is the tube diameter. A mass balance equation for the new variable $N(z,\theta,t)$ is gained by integrating eqn (5) over $\eta\,\mathrm{d}\eta\,\mathrm{d}\varphi\,\mathrm{d}\phi$. Due to the rotational invariance in the cell density distribution, the first two terms in eqn (6), after integrating by parts and utilizing the zero density condition at $\eta = d/2$, are cancelled out with each other. Furthermore, the integration of the integral term in eqn (5) yields

$$\begin{aligned} &\int\int\int\int\int\int p_t(z,\theta',t)\kappa(\eta,\hat{\mathbf{s}}'|\hat{\mathbf{s}})n(\eta,z,\theta', |\phi'-\varphi|,t)\eta\,\mathrm{d}\eta\,\mathrm{d}\varphi\,\mathrm{d}\phi\sin\theta'\,\mathrm{d}\theta'\,\mathrm{d}\phi' \\ &= \int_0^{\pi} p_t(z,\theta',t)K(d,\theta'|\theta)N(z,\theta',t)\sin\theta'\,\mathrm{d}\theta' \end{aligned} \quad (9)$$

with the lumped global turning probability density function $K(d,\theta'|\theta)$ defined to be

$$K(d,\theta'|\theta) = \frac{\int\int\int\int\kappa(\eta,\hat{\mathbf{s}}'|\hat{\mathbf{s}})n(\eta,z,\theta',\varphi,t)\,\mathrm{d}\phi'\,\mathrm{d}\phi\,\eta\,\mathrm{d}\eta\,\mathrm{d}\varphi}{2\pi\int\int n(\eta,z,\theta',\varphi,t)\eta\,\mathrm{d}\eta\,\mathrm{d}\varphi}. \quad (10)$$

If κ is independent of η, as is true in the unbounded bulk, eqn (10) reduces to

$$K(\theta'|\theta) = \frac{1}{2\pi}\int_0^{2\pi}\int_0^{2\pi}\kappa(\hat{\mathbf{s}}'|\hat{\mathbf{s}})\,\mathrm{d}\phi'\,\mathrm{d}\phi \quad (11)$$

which was termed the reduced global turning probability density function in an unbounded

fluid phase by Ford & Cummings (1992). Equation (10) can be viewed as an ensemble-averaged turning probability density function over the cross-section area of the tube.

Normalizing $N(z, \theta, t)$ by the cross-sectional area of the tube and denoting $\bar{n} = 4N/(\pi d^2)$, we obtain

$$\frac{\partial \bar{n}(z, \theta, t)}{\partial t} = -v \cos\theta \frac{\partial \bar{n}(z, \theta, t)}{\partial z} - p_t(z, \theta, t)\bar{n}(z, \theta, t) + \int_0^{\pi} p_t(z, \theta', t)\bar{n}(z, \theta', t) \times K(d, \theta'|\theta)\sin\theta' \, d\theta'. \quad (12)$$

The significance of the mean quantity $\bar{n}(z, \theta, t)$ is removing the azimuthal dependence by integrating over ϕ and φ, which should be expected for the case of cylindrical geometry. Most importantly, $\bar{n}(z, \theta, t)$ also represents an averaged quantity over the radial η. This averaging procedure is often necessary since such information as how the cylindrical wall influences bacterial motion and how this influence impacts the cell density distribution radially is still not available to date. This limitation arises from lack of quantitative knowledge of the various long-range interactions between bacteria and the cylinder wall. If, however, bacteria can be viewed as Brownian particles, we postulate that the bacterial density distribution along the radial direction $n(\eta, z, \theta, t)$ also exhibits the Boltzmann distribution (Brenner & Gaydos, 1977; Deen, 1987) such as,

$$n(\eta, z, \theta, t) = n(0, z, \theta, t)\exp[-E(\eta, \theta)/Q] \quad (13)$$

where $n(0, z, \theta, t)$ represents the density at the tube centerline ($\eta = 0$), $E(\eta, \theta)$ is the sum of various long-range interaction potentials (such as electrostatics and hydrodynamics) in the tube. Since bacteria are mainly self-propelled instead of driven by thermal energy, in the denominator we adopt the bacterial metabolic activity, say Q, which can represent bacterial viability. Accordingly, $\bar{n}(z, \theta, t)$ represents the radial mean by performing the cross-sectional integration,

$$\bar{n}(z, \theta, t) = n(0, z, \theta, t) \times \int_0^{d/2} \exp[-E(\eta, \theta)/Q]\eta \, d\eta \Big/ \int_0^{d/2} \eta \, d\eta. \quad (14)$$

Since a detailed knowledge of the potential field $E(\eta, \theta)$ for bacteria in a tube still remains incomplete, it is impossible at present to evaluate eqn (14) to obtain a more realistic average for $\bar{n}(z, \theta, t)$. For a simple situation such that $E(\eta, \theta) = 0$, i.e. no long-range interactions, the bacterial number density is uniformly distributed along η and $n(\eta, z, \theta, t) = \bar{n}(z, \theta, t)$ exactly.

Equation (12) also is identical to the result derived by Ford & Cummings (1992) who studied the bacterial number density distribution responding to a one-dimensional chemical gradient. Their derivations, though performed in a plane geometry, also are applicable to the axisymmetrical case without considering boundaries since the plane geometry is a special case of the unbounded axisymmetrical geometry.

3. Gas Kinetic Model

In this model some concepts from the rarefied gas dynamics are adopted for bacterial motion and interactions with cylindrical walls. As a result, the derived random motility coefficient in the Fickian flux expression possesses the same harmonic additive structure as the Bosanquet equation. By cross-examining the *a priori* assumptions along with the consequent predictions, we gain a hierarchical understanding regarding the physical implications of the assumptions and, consequently, the potential limitations of the model when applied to bacterial transport.

To conform with the gas kinetic theory, first we assume no long-range interactions between the bacteria and the wall surface, $E(\eta, \theta) = 0$, which means a hard sphere–hard wall model. This leads to $\bar{n}(z, \theta, t) = n(z, \theta, t)$ and $K(d, \theta'|\theta) = K(\theta'|\theta)$. Therefore, bacterial tumbling and turning behaviors within the tube are

the same as in the bulk. Based on the hard sphere–hard wall assumption, one can describe the change in bacterial trajectories due to the wall surface as a collision process. Secondly, we assume that when a bacterium strikes the wall surface, it is temporarily adsorbed and subsequently released from the surface. The short-lived adsorption is assumed to be too small to be noticed compared with typical bacterial run times. Consequently, the collision process is still considered instantaneous. The next running direction after being released from the surface is assumed to be governed by a scattering probability density function that depends on the bacterial incidence angle, $\Upsilon(\theta'|\theta)$.

Given these two assumptions, eqn (5) still applies within the free space of the tube ($\eta < d/2$). On the surface ($\eta = d/2$), appropriate boundary conditions are imposed according to the assumed scattering mechanism. Equation (12) as a result of the radial average over η must also include contributions of those bacteria approaching the impenetrable wall surface and hence being intercepted and scattered back, suggesting that integrating eqn (5) by $\eta\ \mathrm{d}\eta\ \mathrm{d}\varphi\ \mathrm{d}\phi$ should consist of two stages of radial integrations. The first stage of radial integration from $\eta = 0$ to $d/2 - \rho$ results in eqn (12); the second stage of radial integration nearby the tube surface from $\eta = (d/2) - \rho$ to $d/2$ yields the boundary interaction terms. By letting $\rho \to 0$ one obtains

$$\begin{aligned}\frac{\partial n(z,\theta,t)}{\partial t} = &-v\cos\theta\,\frac{\partial n(z,\theta,t)}{\partial z}\\ &- p_t(z,\theta,t)n(z,\theta,t)\\ &+ \int_0^{\pi} p_t(z,\theta',t)n(z,\theta',t)\\ &\times K(\theta'|\theta)\sin\theta'\,\mathrm{d}\theta'\\ &- \frac{4}{d}\frac{v\sin\theta}{\pi}n(z,\theta,t)\\ &+ \frac{4}{d}\int_0^{\pi}\frac{v\sin\theta'}{\pi}n(z,\theta',t)\\ &\times \Upsilon(\theta'|\theta)\sin\theta'\,\mathrm{d}\theta'. \qquad (15)\end{aligned}$$

The factor $4/d$ accounts for the specific wall surface area (surface area per unit tube volume) available for collisions. The term $v\sin\theta/\pi$, similar to the tumbling frequency, is the striking frequency per unit surface area for a specific polar angle θ. This term can be derived easily assuming a uniform density distribution over the cross section of the tube. Due to the projection made by the factor $\sin\theta$, the striking frequency is maximum for θ equal to $\pi/2$, and zero for θ equal to 0 or π. The last integral denotes the θ-summation concerning all such surface collision terms multiplied by a scattering probability density operator $\Upsilon(\theta'|\theta)$ characteristic of the collision mechanism. Note that we have neglected end corrections which is valid only if the tube is sufficiently long.

The radial integration clearly neglected the bacterial excluded volume, which becomes a serious error when d is comparable to the characteristic size of bacteria. Regarding a bacterium as a rigid sphere with a volume-equivalent diameter d_c, the sphere center cannot get any closer to the tube surface than $\eta = (d - d_c)/2$ from a mechanistic point of view. Therefore, only the assumption of zero long-range interactions is critical since we can always define a modified tube diameter $d' = d - d_c$ to account for the excluded volume.

Although an exact solution to eqn (15) is very difficult to obtain, an approximate solution is possible. We (Chen *et al*., 1999) studied eqn (12) in the bulk phase by performing a perturbation analysis on the bacterial density distribution $n(z, \theta, t)$ along the θ direction in terms of a small one-dimensional spatial attractant gradient. In our studies the perturbation in the bacterial angular density distribution was only caused by the anisotropic tumbling frequency induced by the spatial attractant gradient. Our results for the cell subpopulation equations can be directly applied here assuming that the collision terms accounting for the tube boundaries do not interfere with the perturbed cell density solutions, which will be true for a linear equation like eqn (15) and assuming that the wall collision mechanism is independent of chemical gradients. Multiplying eqn (15) by $\sin\theta\ \mathrm{d}\theta$ and integrating over the two half-ranges $0 \sim \pi/2$ and $\pi/2 \sim \pi$,

respectively, two subpopulation cell balance equations for the new dependent variables

$$n^+(z, t) = \int_0^{\pi/2} n(z, \theta, t)\sin\theta \, d\theta \qquad (16a)$$

$$n^-(z, t) = \int_{\pi/2}^{\pi} n(z, \theta, t)\sin\theta \, d\theta \qquad (16b)$$

are rendered. Another related variable is the bacterial density $c(z, t)$ yielded from integrating $n(z, \theta, t)$ over the whole velocity space,

$$c(z, t) = \int_0^{\pi} n(z, \theta, t)\sin\theta \, d\theta$$

$$= n^+(z, t) + n^-(z, t).$$

As to the half-range integrations of the collision terms in eqn (15), analytical evaluation is possible if $\Upsilon(\theta'|\theta)$ is known. However, that is not the intention of this study. Because the structure of the collision terms is generically similar to that of the tumbling terms, it is possible to arrange the outcomes of the integration in groups as $(v/4)[-n^+ + n^-]p_{r,c}$ and $(v/4)[n^+ - n^-]p_{r,c}$, respectively. The quantities $vn^{\pm}/4$ are the number of positive/negative moving bacteria impinging on a unit surface area per unit time, a rather standard result in gas kinetic theory (Kennard, 1938). $p_{r,c}$ represents the averaged one-dimensional reversal probability after collision, as opposed to the reversal probability after tumbling, $p_{r,t}$, which will be introduced shortly. Apparently all inherent complexities are to be combined within $p_{r,c}$. For a simple case assuming a completely diffusive reflection $\Upsilon(\theta'|\theta) = 1/2$ and a uniform cell density distribution $n(z, \theta, t) = c(z, t)/2$, one can easily verify the above grouped expressions with $p_{r,c} = 1/2$.

The final subpopulation balance equations, after integrating eqn (15) according to eqns (16a, b), followed by applying our bulk results (Chen *et al*., 1999), can be arranged in the form of Segel's one-dimensional phenomenological equations by collecting similar terms associated with n^+ and n^-, respectively,

$$\frac{\partial n^+}{\partial t} = -\frac{\partial (v^+ n^+)}{\partial z} - \left\{\left[\tilde{p}_t^+ p_{r,t} + \frac{v}{d} p_{r,c}\right] n^+ - \left[\tilde{p}_t^- p_{r,t} + \frac{v}{d} p_{r,c}\right] n^-\right\}, \qquad (17a)$$

$$\frac{\partial n^-}{\partial t} = \frac{\partial (v^- n^-)}{\partial z} + \left\{\left[\tilde{p}_t^+ p_{r,t} + \frac{v}{d} p_{r,c}\right] n^+ - \left[\tilde{p}_t^- p_{r,t} + \frac{v}{d} p_{r,c}\right] n^-\right\}, \qquad (17b)$$

where v^+ and v^- are the one-dimensional convective velocities, $\tilde{p}_t^+$ and $\tilde{p}_t^-$ the one-dimensional mean tumbling frequencies associated with the positive and negative-moving bacteria, respectively. Their explicit definitions can be found elsewhere (Chen *et al*., 1998). $p_{r,t}$ is the one-dimensional reversal probability due to the tumbling (Rivero *et al*., 1989; Chen *et al*., 1998, 1999) defined by

$$p_{r,t} = \frac{1 - \psi}{2}. \qquad (18)$$

Equations (17a, b), first proposed by Barton & Ford (1997), resemble the one-dimensional phenomenological cell balance equations of Rivero *et al*. (1989), except now the *overall* reversal frequencies (represented by the terms in square brackets), $P^+ = \tilde{p}_t^+ p_{r,t} + (v/d)p_{r,c}$ and $P^- = \tilde{p}_t^- p_{r,t} + (v/d)p_{r,c}$ are the linear sum of the tumbling and the collision contributions. Note that the tumbling terms are not influenced by d, while the collision terms are linearly added as corrections for the inclusion of solid boundaries. Such a pleasant additive structure results from the assumptions that we still view the bacterial tumbling as a valid Poisson process and that the turning behavior remains unchanged within the free space of the capillary tube. Simply stated, tumbling and collision are mutually independent.

Adding both eqns (17a) and (17b) together and subtracting one from the other, two partial differential equations (PDEs) in terms of the

number density $c(z, t)$ and the bacterial net flux $J(z, t)$,

$$J(z,t) = v\int_0^{\pi} n(z, \theta, t)\cos\theta \sin\theta \, d\theta, \quad (19)$$

in the z-direction are obtained. Following Segel's reasoning and invoking the steady-state flux assumption, a pseudo-equilibrium bacterial flux is obtained in the Fickian form of the Keller & Segel (1971) model as

$$J(z,t) = -\nabla_z[\mu_d c(z,t)] + V_c \cdot c(z,t) \quad (20)$$

where the random motility coefficient μ_d and the chemotactic velocity V_c (analogous to the molecular self-diffusion coefficient and to the bulk convective velocity, respectively) are given by

$$\mu_d = \frac{v^2}{3p_1(1-\psi)}\left(\frac{1}{1+\mathrm{Kn}\dfrac{p_{r,c}}{p_{r,t}}}\right) \quad (21)$$

and

$$V_c = \frac{\xi v}{3}\left(\frac{1}{1+\mathrm{Kn}\dfrac{p_{r,c}}{p_{r,t}}}\right) \quad (22)$$

in which ξ is defined (Chen, 1997; Ford & Cummings, 1992) as

$$\xi(z,t) = vv\frac{dN_b}{da}\frac{\partial a(z,t)}{\partial z}$$

with v (s receptors^{-1}) representing a sensitivity factor, N_b the bound receptors per bacterium, and a the chemical attractant concentration.

3.1. MODEL PREDICTIONS

When the tube diameter is extremely large compared with the bacterial mean run length ($\mathrm{Kn} \ll 1$) such that $\mathrm{Kn}(p_{r,c}/p_{r,t}) \ll 1$, eqn (21) yields the same expression as μ^o in eqn (1). At the other limit $\mathrm{Kn} \gg 1$ such that $\mathrm{Kn}(p_{r,c}/p_{r,t}) \gg 1$, eqn (21) asymptotically reaches the Knudsen diffusivity,

$$\lim_{(\mathrm{Kn}\to\infty)} \mu_d = \frac{vd}{3}\frac{1}{2p_{r,c}}, \quad (23)$$

which further yields the usual gas kinetic expression $vd/3$ provided that $p_{r,c} = 1/2$. Comparing eqn (23) with (3) suggests that $p_{r,c}$ can be related to f, the fraction of rebound bacteria undergoing diffusive reflection, by

$$p_{r,c} = \frac{1}{2}\frac{f/2}{(1-f/2)}. \quad (24)$$

By now it is obvious that eqn (21) is actually the Bosanquet equation that predicts a harmonic average of μ_d from both limiting values over a wide range of Kn, an outcome that should be expected since the essence of Bosanquet's assumption—the overall transport resistance being the sum of both automatic tumbling and cell–wall collisions resistances—is preserved in eqn (15). The derivation of μ_d in the form of the Bosanquet equation is not just a mathematical manipulation but a correct depiction of the *linear* transport phenomena in gas kinetic theory. It is well-accepted that the most direct and general approach to modeling combined bulk and Knudsen diffusion in a multi-component mixture is the "dusty gas theory" (Froment & Bischoff, 1979). The Bosanquet formula posed as the overall diffusion coefficient of any component in the mixture can be derived via straightforward application of the generalized Maxwell–Stefan relations (Krishna & Weeselingh, 1997) which also is built upon the *linear* transport theory. Linearity in the transport resistance is the key ingredient in derivations leading to the Bosanquet equation.

It is interesting to note that the same harmonic form also applies to the chemotactic velocity V_c. When $d \to \infty$, the asymptotic result $\xi v/3$ is simply a restatement of the bulk result in Chen *et al*. (1998a). When $d \to 0$, V_c decreases to zero, which can be understood by recognizing that at large Kn the dominating turning mechanism becomes the cell–wall collisions independent of the spatial chemical gradient. Note that the bulk values are the upper limits for μ_d and V_c regardless of $p_{r,c}$. If $p_{r,c} = 0$ ($f = 0$), the one-dimensional transport mechanism does not differ from that in the bulk because the z-component velocity is not altered before and after a collision. In Fig. 2 the common harmonic relationship $[1 + \mathrm{Kn}(p_{r,c}/p_{r,t})]^{-1}$ is plotted vs. Kn for various values of f. General trends are that increasing f will decrease both transport parameters (μ_d and V_c), and smaller values of f delay

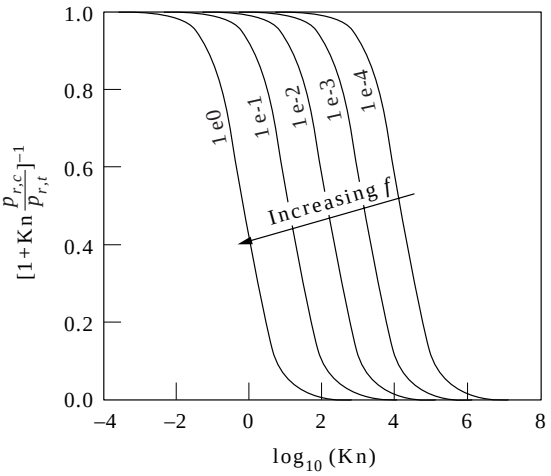

FIG. 2. The common harmonic factor in eqns (21)–(22) vs. $\log_{10}$ (Kn) for various values of f, assuming $p_{r,t} = 1/2$.

the beginning of the decay of the transport parameters to larger Kn.

Although the gas kinetic model provides a theoretical basis for the appropriate chemotactic velocity to be used in conjunction with the Bosanquet equation for the diffusion coefficient, the prediction does not appear to agree with experimental results (Berg & Turner, 1990). This is because the derivations leading to eqns (21) and (22) are only valid when a bacterium is not constrained to move in a certain way by the restrictive geometry. The bacterium is assumed to be free to turn into any direction after a tumble or collision. Clearly, the uniform cell angular density distribution resulting from the hard sphere–hard wall assumption is unable to mimic the swimming behavior of bacteria *E. coli* in small capillaries. According to Liu & Papadopoulos (1995), the presence of the tube walls can interfere with bacterial turning behavior by confining the turning to geometrically favorable directions, which is the so-called "guidance of the straight tube" reported by (Berg & Turner, 1990). To remedy this shortcoming of our model equations, in the next section we propose another model, which focuses on the variation of the global turning probability distribution and the bacterial swimming orientations with tube diameter.

4. Orientation Model

The microscopic observations of Liu & Papadopoulos (1995) and the macroscopic migration measurements of Berg & Turner (1990) suggest that in a small capillary the probability of swimming along the tube is greater than swimming crosswise. In other words, the bacterial number density distribution in directional space is elongated towards both ends of the tube axis. This distorted distribution resembles the shape of a dumbbell and deviates significantly from the pseudo-uniform density distribution assumed in the bulk phase. Since the swimming speed and the tumbling frequency do not change considerably subject to the restrictive geometry (Liu & Papadopoulos, 1996; Phillips, 1992), such a distortion in the angular density distribution may arise from interference with the bacterial turning mechanism by geometrical constraints. A connection must exist, therefore, between the bacterial turning probability density distribution and the tube diameter. By the definition of the bacterial bulk density, we assume that the bacterial angular number density can be written as $\bar{n}(z, \theta, t) = c(z, t)\Omega(\theta, t)$ where $\mathbf{\Omega}(\theta, t)$ is required to satisfy $\int_0^\pi \Omega(\theta, t)\sin\theta \, \mathrm{d}\theta = 1$. The dependence of Ω on position z is usually unimportant and can be ignored or incorporated into t by employing a Lagrangian approach. The normalized coefficient function Ω, termed the *orientation distribution function* is of great importance because of its direct influence on the bacterial random and biased motilities.

4.1. THE TURNING PROBABILITY DENSITY FUNCTION (PDF)

In an unbounded phase the stochastic turning probability density function is only dependent upon the turn angle $\alpha(=\cos^{-1}\hat{\mathbf{s}}'\cdot\hat{\mathbf{s}})$ between any two successive swimming vectors. This local turning probability density function, $W(\alpha)$, is usually determined experimentally. A general methodology of converting $W(\alpha)$ into the global turning probability density function $K(\theta'|\theta)$ has recently been proposed by us (Chen *et al.*, 1998). Comparisons of theoretical approximations with experimental data for $W(\alpha)\sin\alpha$ are shown in Fig. 3(a). Two important properties

of $K(\theta'|\theta)$ in the bulk phase are that the two angular integrations

$$\int_0^{\pi} K(\theta'|\theta)\sin\theta\,\mathrm{d}\theta = 1 \qquad (25a)$$

$$\int_0^{\pi} K(\theta'|\theta)\sin\theta\cos\theta\,\mathrm{d}\theta = \psi\cos\theta' \qquad (25b)$$

are satisfied (Chen *et al*., 1998) irrespective of the explicit form of $K(\theta'|\theta)$. The first equation derives from the turning probability conservation over the velocity space; the second indicates the bacterial directional persistence, ψ, relative to the preceding swimming vector in the three-dimensional space.

When in a geometrically-restricted environment, the adoption of the local turning probability distribution becomes inconvenient due to its variations with location and swimming orientation. Directly employing the global turning probability density distribution $K(d, \theta'|\theta)$ is conceptually simpler for relating to the observed over-all turning behavior. The philosophy of this turning model lies in the idealization that in a cylindrical tube of diameter d, a gap in the bacterial global turning probability density distribution $K(d, \theta'|\theta)$ centered around $\theta = \pi/2$ occurs as d decreases down to a certain value comparable to the flagellar length. The gap in which the bacterial turning probabilities are excluded broadens as d monotonically decreases. The exclusive angle range $(\theta_d, \pi - \theta_d)$ is the combined consequence of steric restriction and various long-range interactions. θ_d is assumed to have a one-to-one mapping relationship with the tube diameter.

The probability distribution along θ pertaining to the other regions $[0, \theta_d]$ and $[\pi - \theta_d, \pi]$ is assumed to be uniform. To satisfy the asymptotic

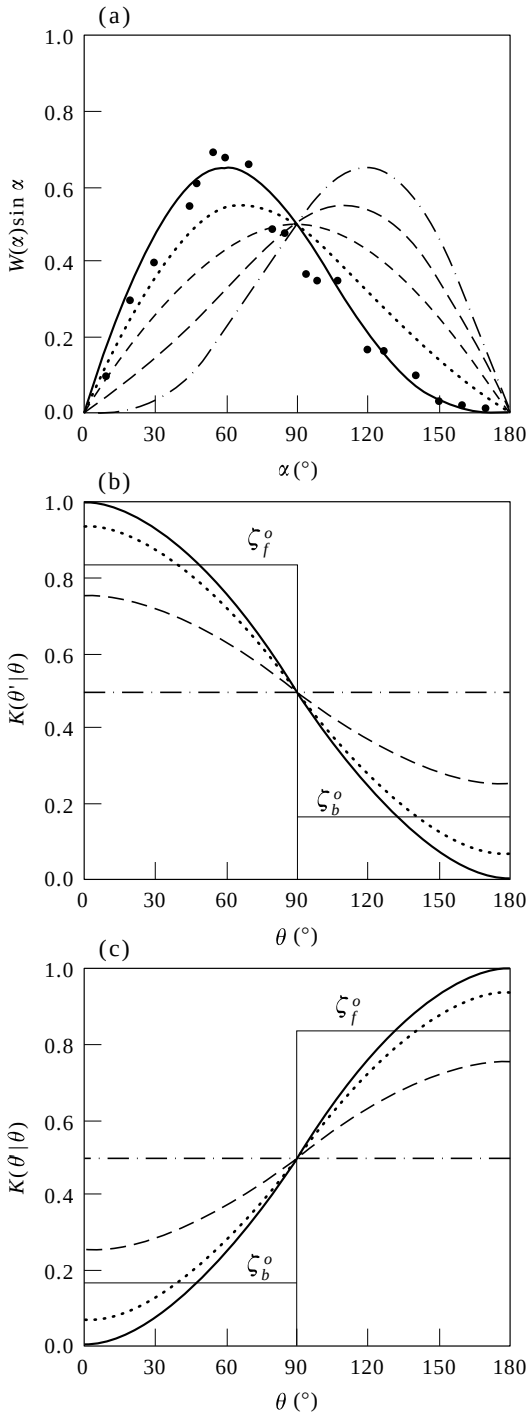

FIG. 3. Conversion of a local turning PDF $W(\alpha)$ to a global turning PDF $K(\theta'|\theta)$: (a) comparisons of an experimentally determined turning PDF for *E. coli* (● from Berg & Brown, 1972) with curve-fits to a first-order polynomial in $\cos\alpha$ for a range of $\psi = \langle\cos\alpha\rangle$ values: (—) 1/3; (· · · ·) 1/6; (- - -) 0; (– –) −1/6; (– - –) −1/3. The best fit was given by $\psi = 1/3$. The local PDF from (a) is mapped to a global PDF for values of θ' which range from 0 to 90 in (b): (—) 0; (· · · ·) 30; (– –) 60; (- - -) 90 and 90 to 180 in (c): (– - –) 90; (- -) 120; (· · · ·) 150; (—) 180; those continuous functions can be approximated by step-like, discontinuous lines. The magnitude of the steps is therefore a function of θ'. (b) for $\theta' = 0$, the corresponding discontinuous approximation is shown with a solid line. (c) for $\theta' = 180$, the corresponding discontinuous approximation is shown with a solid line. Values of ς_f^0 and ς_b^0 for the discontinuous functions were 5/6 and 1/6, respectively, when $\psi = 1/3$.

condition at the bulk extreme, $\lim_{d\to\infty}\theta_d = \pi/2$, the discontinuous uniform probability distribution also is extended to the unbounded bulk with the two means $h^o(\theta')$ and $g^o(\theta')$ that are selected to approximate the original smooth distribution. The superscript ^{o} indicates quantities in the unbounded bulk phase. This discontinuous turning probability density function $K(\theta_d, \theta'|\theta)$ in a tube of an arbitrary diameter is given as

$$K(\theta_d, \theta'|\theta) = \begin{cases} h(\theta_d, \theta'), & \theta \in [0, \theta_d] \\ 0, & \theta \in (\theta_d, \pi - \theta_d) \\ g(\theta_d, \theta'), & \theta \in [\pi - \theta_d, \pi] \end{cases} \tag{26}$$

in which

$$h(\theta_d, \theta') = \frac{1}{2}\{[\varsigma_f(\theta_d) + \varsigma_b(\theta_d)] + [\varsigma_f(\theta_d) - \varsigma_b(\theta_d)]\cos\theta'\} \tag{27a}$$

$$g(\theta_d, \theta') = \frac{1}{2}\{[\varsigma_f(\theta_d) + \varsigma_b(\theta_d)] - [\varsigma_f(\theta_d) - \varsigma_b(\theta_d)]\cos\theta'\} \tag{27b}$$

and where the subscripts $_f$ and $_b$ indicate the forward and backward turning motion for the turning probability density, respectively. Forward turning refers to the situations when cosines of θ' and θ are of the same sign, as opposed to the backward turning in which $\cos\theta'$ and $\cos\theta$ have the same opposite signs. In eqns (27a) and (27b) the forward and backward turning motion agrees with the preceding swimming direction θ' in the sense that $h(\theta_d, 0) = \varsigma_f(\theta_d)$ and $g(\theta_d, 0) = \varsigma_b(\theta_d)$ at $\theta' = 0$; whereas $h(\theta_d, \pi) = \varsigma_b(\theta_d)$ and $g(\theta_d, \pi) = \varsigma_f(\theta_d)$ at $\theta' = \pi$. In Fig. 3(b)–(c) the continuous global turning probability density distribution function $K(\theta'|\theta)$ for *E. coli* in the bulk phase is plotted vs. θ at various values of the preceding running angle θ'. The discontinuous approximations for $K(\theta'|\theta)$ also are displayed as comparisons for $\theta' = 0$ and π. In both cases $\varsigma_f(\theta_d)$ and $\varsigma_b(\theta_d)$ reduce to ς_f^o and ς_b^o, respectively.

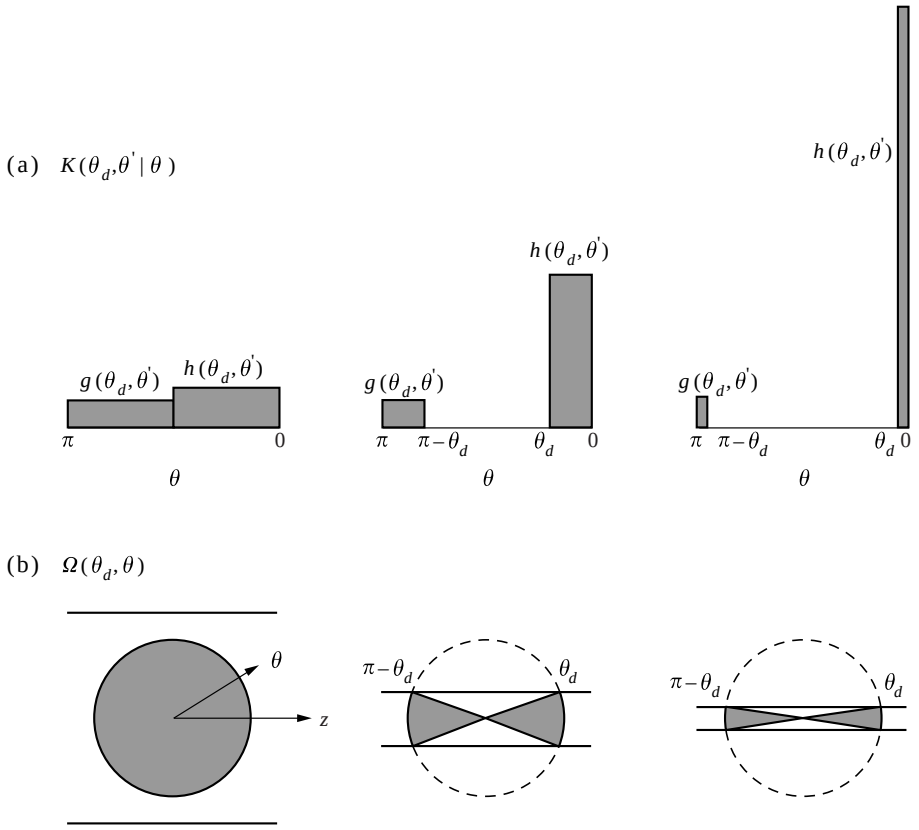

FIG. 4. Conceptual diagrams showing (a) the discontinuous global turning probability density distributions and (b) the corresponding orientation functions at three different tube diameters.

This turning model for $K(\theta_d, \theta'|\theta)$ is depicted in Fig. 4 to demonstrate how the simplified discontinuous global turning probability density distribution evolves with d. The question of the existence of such a gap is by all means the hardest to settle. The realistic global turning probability distribution along θ may be smooth and continuous with a minimum well instead of an obvious gap. At present, however, it is rather appropriate to make simple approximations and explore its impact on the macroscopic transport behavior. Information extracted from this approximation will provide at least an initial basis for predicting bacterial running and turning behaviors in a capillary tube both at microscopic and macroscopic levels. Similar to $K(\theta_d, \theta'|\theta)$, θ_d also represents the ensemble-averaged parameter over the cross section of the tube. The deflection of bacterial trajectories close to the wall surfaces also is accounted for in the parameter θ_d. The dependence of $\varsigma_f(\theta_d)$ and $\varsigma_b(\theta_d)$ on θ_d results from the two similar integrations,

$$\int_0^{\pi} K(\theta_d, \theta'|\theta)\sin\theta \, \mathrm{d}\theta = 1, \qquad (25a')$$

$$\int_0^{\pi} K(\theta_d, \theta'|\theta)\sin\theta\cos\theta \, \mathrm{d}\theta = \varpi(\theta_d)\cos\theta'. \qquad (25b')$$

The second integration, motivated by eqn (25b) in the bulk phase, characterizes the unbalanced probability distribution between $h(\theta_d, \theta')$ and $g(\theta_d, \theta')$ within the tube. At the limit $\theta_d \to \pi/2$, $\varpi(\theta_d) \to \psi$ and eqn (25b′) reduces back to (25b).

Substituting eqn (26) into eqns (25a′) and (25b′) yields

$$\varsigma_f(\theta_d) + \varsigma_b(\theta_d) = \frac{1}{1-\cos\theta_d} \geqslant 1 \qquad (28)$$

and

$$\varsigma_f(\theta_d) - \varsigma_b(\theta_d) = \frac{2\varpi(\theta_d)}{1-\cos^2\theta_d} \geqslant 0 \qquad (29)$$

respectively. As $\theta_d \to \pi/2$, ς_f and ς_b recover back to their bulk values, ς_f^o and ς_b^o. We also assume that $\varsigma_f \geqslant \varsigma_b$, implying that $\varpi(\theta_d)$ must be non-negative.

4.2. ORIENTATION DISTRIBUTION FUNCTION

Having determined a global turning PDF, we now proceed to develop the equilibrium bacterial orientation distribution function subject to a specific tube diameter. Assume that a long cylindrical tube of large diameter is initially filled with a uniform bacterial suspension. At $t = 0$, d suddenly shrinks to a much smaller value such that a gap in the discontinuous global turning probability density function appears. Then the transient bacterial orientation distribution function $\Omega(\theta, t)$ subject to the sudden shrinkage in the tube diameter can be analysed by eqn (12). Designate the region $(\theta_d, \pi - \theta_d)$ in which the bacterial swimming directions are conceptually normal to the tube axis the N-region, and the other two regions $[0, \theta_d]$ and $[\pi - \theta_d, \pi]$ in which the swimming directions are conceptually parallel to the tube axis the P-regions. Then we name the orientation distribution function in the N-region as $\Omega_\perp(\theta, t)$, and in the other two P-regions as $\Omega_=(\theta, t)$. Substituting the unknown $\Omega_\perp$ and $\Omega_=$ and the constant p_t in eqn (12) yields

$$\frac{\mathrm{d}\Omega_\perp(\theta, t)}{\mathrm{d}t} = -p_t\Omega_\perp(\theta, t), \quad \Omega_\perp(\theta, t) = \frac{1}{2} \, @t = 0 \qquad (30)$$

and

$$\frac{\mathrm{d}\Omega_=(\theta, t)}{\mathrm{d}t} = p_t\cos\theta_d(\varsigma_f + \varsigma_b)\Omega_\perp(\theta, t),$$

$$\Omega_=(\theta, t) = \frac{1}{2} \, @t = 0 \qquad (31)$$

which have the solutions

$$\Omega_\perp(\theta, t) = \frac{1}{2}\exp[-p_t t], \qquad (32)$$

$$\Omega_=(\theta, t)$$

$$= \frac{1}{2}\{1 + \cos\theta_d(\varsigma_f + \varsigma_b)[1 - \exp(-p_t t)]\}. \qquad (33)$$

Thus $\Omega_\perp$ in the N-region decreases exponentially with time in compensation for the increases of $\Omega_=$ in the two P-regions. $\Omega_=$ is equally distributed in both P-regions since we have not considered spatial chemical gradients yet. Generally, only

the equilibrium bacterial density distribution is of interest. Hence $\Omega_{\perp}(\theta,\infty) = 0$, and

$$\Omega_{=}(\theta,\infty) = \frac{1}{2}\frac{1}{(1-\cos\theta_d)} \geqslant \frac{1}{2} \tag{34}$$

upon substituting eqn (28) for $\varsigma_f + \varsigma_b$. Note that $0 \leqslant \theta_d \leqslant \pi/2$ so that $\cos\theta_d$ cannot be negative. This is the anticipated equilibrium result: bacteria in the P-regions cannot turn into the N-region, whereas bacteria previously in the N-region must turn out into the P-regions. Given a sufficient time, $\Omega_{\perp}$ decreases to zero.

Using the equilibrium orientation distribution function in eqn (34) as the initial condition, we next explore the impact of the anisotropic tumbling frequency p_t perturbed by the spatial chemical gradient on $\Omega_{=}$. The perturbation approach that follows is adopted from Chen *et al*. (1999). Assume at $t = t_0$ a constant one-dimensional spatial chemoattractant gradient (characterized by $\xi > 0$ for an attractant gradient) is uniformly imposed everywhere within the tube, anisotropically perturbing the tumbling frequency based on $\xi\cos\theta$. If the chemical gradient is small enough, p_t can be approximated by a linear expansion

$$p_t(z,\theta,t_0+t) = p_1(z,t)[1-\xi\cos\theta] + O(\xi^2)$$

about the small parameters ξ. Then the bacterial orientation distribution function $\Omega_{=}(z,\theta,t_0+t)$ perturbed by the small parameter ξ can be evaluated by substituting eqn (34) for $\Omega_{=}(z,\theta,t_0)$ and the linearly expanded p_t into eqn (12). The perturbed results for both P-regions can be written in compact form as

$$\Omega_{=}(z,\theta,t_0+t) = \frac{1}{2(1-u_d)}\left\{1 + \Omega^1_{=} \times \left[\cos\theta - \mathrm{Sgn}(\cos\theta)\frac{2(1-u_d^3)}{3(1-u_d^2)}\varpi(u_d)\right]\xi\right\} + O(\xi^2\cos^2\theta) \tag{35}$$

in which $\cos\theta_d$ is replaced by the symbol u_d hereafter for simplicity. $\mathrm{Sgn}(\cos\theta) = 1$ for $\theta \in [0,\theta_d]$ and $\mathrm{Sgn}(\cos\theta) = -1$ for $\theta \in [\pi-\theta_d,\pi]$. $\Omega^1_{=}$ is the expansion coefficient and is solved as

$$\Omega^1_{=}(z,t_0+t) \doteq 1 - \exp\left[-\int_{t_0}^{t} p_1(z,t')Dt'\right]. \tag{36}$$

which gives an equilibrium value of one given a characteristic time of the order p_1^{-1}.

4.3. PHYSICAL CONSTRAINTS

Examining the orientation function in eqn (35) reveals a physical constraint bounding the reasonable values of $\varpi(u_d)$. Since $\xi > 0$, one expects $\Omega_{=}$ to be larger in the region $[0,\theta_d]$ and smaller in the region $[\pi-\theta_d,\pi]$ than the equilibrium value $1/[2(1-u_d)]$, such that a net positive flux of the bacterial population along the positive z direction is observed. Thus in view of eqn (35), $\varpi(u_d)$ must be confined within the inequality relation

$$0 \leqslant \varpi(u_d) \leqslant \frac{3u_d(1-u_d^2)}{2(1-u_d^3)} \tag{37}$$

to ensure such a physical sense.

Because we assume that the restrictive geometry only increases the directional persistence, $\varpi(u_d)$ is always larger than its bulk value ψ. This is based on the idea that in a small capillary bacteria cannot turn backward more often than in bulk phases. However, as θ_d approaches $\pi/2$, $u_d \to 0+$ and ϖ inevitably becomes zero due to the loss of its upper bound. $\varpi(0) = 0$ means $\varsigma_f^o - \varsigma_b^o = 0$, implying that the global turning probability density function in the unbounded bulk must be a *continuous* one and, in this case, a uniform one as well. Thus our current model is only applicable to motile bacteria exhibiting zero directional persistence in the bulk phase. To make the model also applicable to the case when $\psi \neq 0$, the approximate functions h and g in eqn (26), instead of being constants over θ, should be modified to be polynomials of $\cos\theta$. However, we are not concerned with pursuing this complexity herein. The upper and lower bounds of eqn (37) are shown in Fig. 5(a). It is not known at present how $\varpi(u_d)$ varies specifically with u_d except the bounding relation eqn (37). Thus we study the two limiting situations: $\varpi(u_d)$ is equal to its upper and lower bounds, respectively. All the derived results that follow are summarized in Table 1.

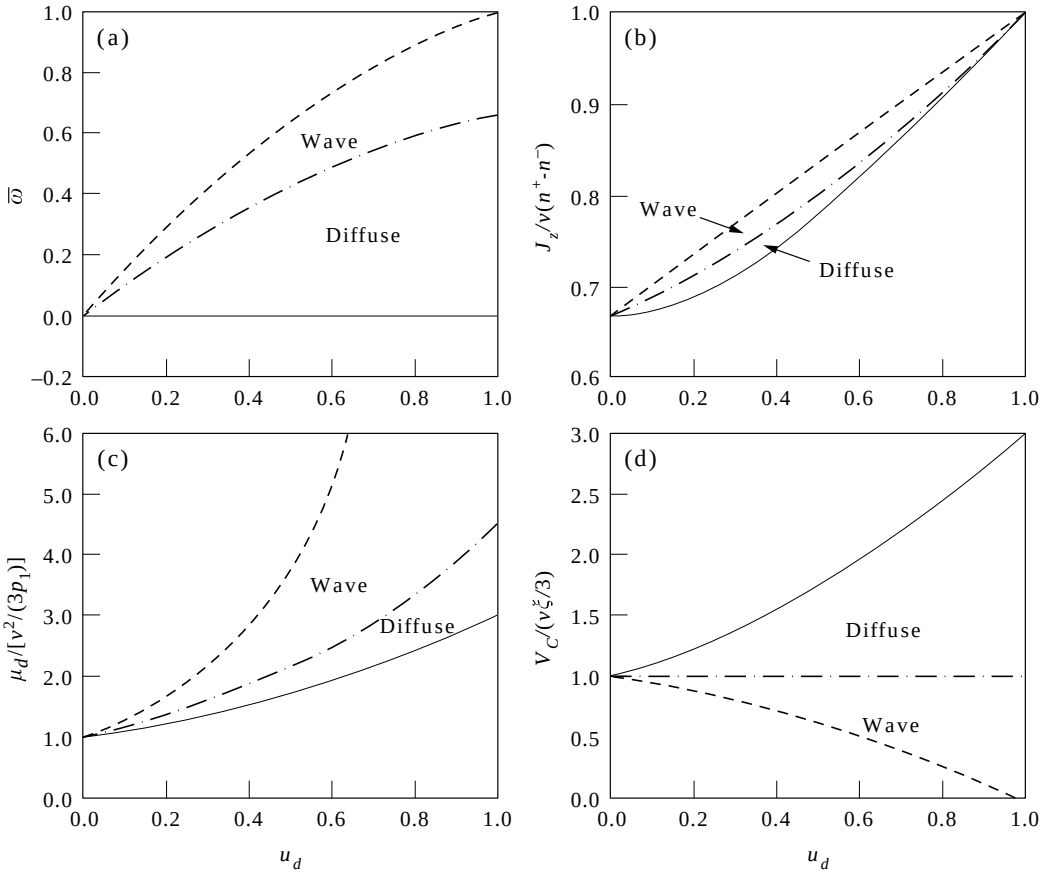

FIG. 5. Theoretical bounding lines subject to the upper bounds (- - -), lower bounds (—), and the middle lines (– - –) of ϖ for (a) ϖ, (b) flux ratio, (c) dimensionless μ_d and (d) dimensionless V_c vs. u_d. Note that V_c predicted by the upper bound of ϖ is lower than that predicted by the lower bound of ϖ.

4.4. UPPER BOUNDS

Assuming $\varpi(u_d)$ is always equal to its upper bound, then $\varpi \to 1$ and $\varsigma_f - \varsigma_b \to +\infty$, as $u_d \to 1$. This means in an extremely small capillary the backward probability density $\varsigma_b \to 0$ and the forward probability density $\varsigma_f \to +\infty$. The prediction of zero reverse turning qualitatively agrees with the swimming behavior of *E. coli* in a 3 μm capillary observed by Liu *et al*. (1997): an individual bacterium continuously swam forward in the axial direction and

TABLE 1
Analytical expressions of various results for the upper, lower bounds and the middle lines

	Upper bounds		Lower bounds		Middle	
ϖ	$\frac{3u_d(1-u_d^2)}{2(1-u_d^3)}$	(38a)	0	(39a)	$\frac{u_d(1-u_d^2)}{(1-u_d^3)}$	(40a)
$\frac{J}{v(n^+-n^-)}$	$\frac{2+u_d}{3}$	(38b)	$\frac{2(1-u_d^3)}{3(1-u_d^2)}$	(39b)	$\frac{2}{3-u_d}$	(40b)
$\frac{\mu_d}{v^2/(3p_1)}$	$\frac{(2+u_d)(1+u_d)}{2(1-u_d)}$	(38c)	$1+u_d+u_d^2$	(39c)	$\frac{(1+u_d)}{(1-u_d/3)^2}$	(40c)
$\frac{V_c}{v\xi/3}$	$\frac{(2+u_d)(1-u_d)}{2}$	(38d)	$1+u_d+u_d^2$	(39d)	1	(40d)

rarely turned backward. This forward swimming phenomenon is attributed to a steric limitation which, in fact, has been implicitly incorporated in our global turning model. Two implications for an infinitely large forward probability density and a zero backward probability density when $\varpi(u_d = 1) = 1$ are: (i) the bacterial macroscopic transport ceases to be diffusional and, instead, resembles a wave motion; and (ii) no chemotaxis is exhibited even in the presence of attractant gradients.

Using the definitions of eqns (16a, b), $n^+(z, t)$ and $n^-(z, t)$ can be obtained by integrating each orientation distribution function over the corresponding P-region. The bacterial net flux in the z-axis is obtained according to eqn (19). Considering only the leading terms, the ratio of J to $v(n^+ - n^-)$ is given by eqn (38b) in Table 1, which states that J actually equals $v(n^+ - n^-)$ (a one-dimensional definition as in Segel, 1977) when $\theta_d = 0$, and $J = \frac{2}{3}v(n^+ - n^-)$ (a three-dimensional result as in Chen *et al*., 1999) when $\theta_d = \pi/2$. Utilizing eqns (25a′) and (25b′) and integrating eqn (12) by $\sin\theta\ \mathrm{d}\theta$ over all θ again gives the mass conservation equation for the bacterial density $c(z, t)$

$$\frac{\partial c(z, t)}{\partial t} = -\frac{\partial J(z, t)}{\partial z}. \tag{41}$$

Following Segel's approach (Segel, 1976, 1977) and utilizing eqn (38b), a differential equation for the bacterial net flux is obtained as

$$\frac{\partial J}{\partial t} = -\frac{v^2}{2}\frac{(2 + u_d)(1 + u_d)}{3}\frac{\partial c}{\partial z} - p_1(1 - u_d)J + p_1\left(\frac{v\xi}{3}\right)\frac{(2 + u_d)(1 - u_d)^2}{2}c \tag{42}$$

which for a long elapsed time $t \gg [p_1(1 - u_d)]^{-1}$ yields a pseudo-equilibrium flux expression in the Fickian form of eqn (20) with the random motility coefficient and the chemotactic velocity now explicitly expressed as eqns (38c) and (38d). Substituting the Fickian flux back into eqn (41) then yields a diffusion equation with a bulk flow term. One thing to note is the validity of the pseudo-equilibrium flux expression that is built on the time-scale $t \gg [p_1(1 - u_d)]^{-1}$. When u_d tends to unity, a remarkably large diffusion coefficient can be yielded only if the waiting time is sufficiently long. If the waiting time is not long enough, the exhibited transient macroscopic motion is wavelike (Othmer *et al*., 1988).

The expected asymptotic behavior from eqn (38c) is that $\mu_d \to \mu^o$ as $u_d \to 0+$, i.e. when the tube diameter is sufficiently large. We also notice that $\mu_d \to +\infty$ when $u_d \to 1-$. The physical implication of an infinitely large diffusion coefficient is that the net flux is so large that the macroscopic bacterial transport process ceases to be diffusional. In fact, at $u_d = 1$, results like eqns (38c, d) cannot be valid, for the pseudo-equilibrium is never established within the time scale of interest. Reexamining the partial differential equation (42) finds that the last two terms of eqn (42) become zero at $u_d = 1$. Under this circumstance, substituting eqn (42) into eqn (41) yields the one-dimensional wave equation

$$\frac{\partial^2 c}{\partial t^2} = v^2\frac{\partial^2 c}{\partial z^2} \tag{43}$$

which is of hyperbolic form with a constant wave speed v, and the mass c is constant along the families of the characteristics $\zeta = z \pm vt$.

The transition between wave-like motion and a diffusional process is dependent upon the time/length-scale. For the case of bacterial movement within a capillary, the corresponding cell transport behavior will remain diffusional provided that the length of the capillary is sufficiently long to allow a bacterium the chance to turn backward after a series of consecutive forward turnings before reaching one end of the tube. If the capillary is not long enough for a bacterium starting at one end of the capillary to turn backward at least once before reaching out of the other end, what is observed is wave-like movement, as seen by Liu *et al*. (1997).

4.5. LOWER BOUND

Next we rederive the above results by assuming $\varpi(u_d) = 0$, which means that the directional persistence within a tube, no matter how narrow it is, retains the same value ($\psi = 0$) as in the bulk. Repeating the derivation procedure again, we found that the flux ratio now yields eqn (39b) which predicts lower values than eqn (38b), but agrees with eqn (38b) at both extremes ($u_d = 0$ and $u_d = 1$). In a similar

manner, the pseudo-equilibrium flux is derived and found to have a characteristic relaxation time p_1^{-1} that is independent of u_d. The resulting μ_d and V_c are given as eqns (39c, d) in Table 1. Note that eqn (39c) always predicts a finite random motility coefficient since $\varpi(u_d)$ in this case retains its bulk value. Of particular interest is that as u_d varies from zero to 1, μ_d and V_c transiently change from their three-dimensional results in the bulk previously derived by Chen *et al*. (1999) to the one-dimensional expressions proposed by Rivero *et al*. (1989), respectively. In other words, only the dimensionality changes.

The various theoretical predictions based on the upper and lower bounds of $\varpi(u_d)$ are plotted in Fig. 5. Results derived from the upper bounds and the lower bounds of $\varpi(u_d)$ are drawn in dashed and solid lines, respectively. The dot–dashed lines represent the corresponding results (as in the 3rd column of Table 1) for $\varpi(u_d)$ being equal to two-thirds of the upper bounds, which will be introduced shortly. Due to the monotonic one-to-one mapping relation, all physically reasonable quantities must fall between the two bounding lines as depicted. Figure 5(b) shows the flux ratios according to the results in Table 1. Both predictions meet each other at $u_d = 0$ and $u_d = 1$. The dimensionless random motility coefficients scaled by the bulk expression $v^2/(3p_1)$ are depicted in Fig. 5(c), in which the upper bound goes to positive infinity as $u_d \to 1$. Conversely, in Fig. 5(d) the theoretical line predicted by the upper bound of ϖ becomes the lower bound for V_c, and approaches zero at $u_d = 1$. Both lines only converge in the bulk phase ($u_d = 0$).

All the predictions are physically reasonable, recalling that the bacteria with a totally suppressed backward turning probability have a wave transport pattern, but are unable to exhibit chemotaxis even though the tumbling frequency still responds to the spatial chemical gradient. Such a conclusion certainly rests upon a tacit assumption: the tumbling frequency is not the *only* biological response influenced by the chemical gradients. If, say, the swimming speed v is higher than a basal value whenever the bacterium is swimming up an attractant gradient, one can still observe an enhanced transport rate at the end of an extremely narrow capillary which is connected to the attractant source, even though the cellular motion now is a typical wave propagation. Although the swimming speed of *E. coli* was found to increase up to 40% over the basal value in incubation when the attractant serine was added (Berg & Brown, 1972; Phillips *et al*., 1994), it is doubtful that the response is instantaneous.

Physically, V_c is allowed to either increase or decrease with u_d without violating eqn (37). These opposite trends in the upper and lower bounds exhibited by the variations of V_c with u_d in Fig. 5(d) help us judge whether the bacterial transport mode in capillaries is closer to either a wave or diffusive mode, thus further narrowing the possible range for $\varpi(u_d)$. When $\varpi(u_d)$ is set equal to $u_d(1 - u_d^2)/(1 - u_d^3)$, the chemotactic velocity remains independent of u_d at its bulk value. This is because the reduction in dimensionality is exactly counter-balanced by the increase of the directional persistence. If $\varpi(u_d)$ crosses over the middle line in Fig. 5(a), the trend of V_c along u_d reverses.

Note that results in Fig. 5(c) are scaled by the non-persistent random motility coefficient in the bulk, which is only appropriate for the lower bound of μ_d, but not for others that include directional persistence. Regardless of the equilibrium time, we scale μ_d in eqns (38c) and (40c)

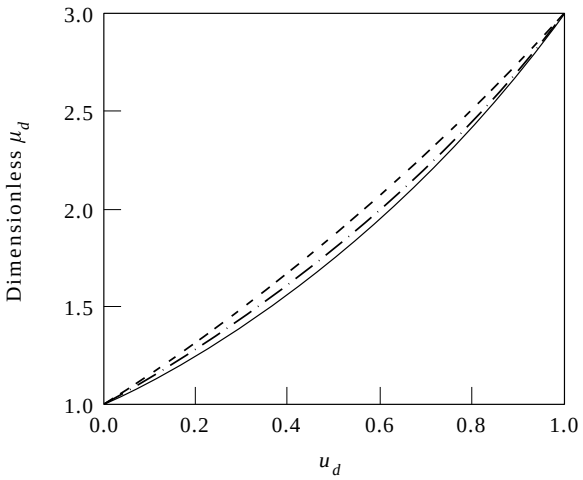

FIG. 6. Replot of Fig. 5(c) with the dimensionless random motility coefficient normalized by its own equilibrium expression: (—) eqn (39c); (– - –) eqn (40c′); (- - -) eqn (38c′).

by including their own directional persistence factors,

$$\frac{\mu_d}{v^2/[3p_1(1-u_d)]} = 1 + \frac{3}{2}u_d + \frac{1}{2}u_d^2, \quad (38c')$$

$$\frac{\mu_d}{v^2/[3p_1(1-u_d/3)]} = \frac{(1+u_d)}{(1-u_d/3)}. \quad (40c')$$

The scaling factors $(1-u_d)$ and $(1-u_d/3)$ above, similar to $(1-\psi)$ in eqn (1), are the corresponding factors in the one-dimensional reversal probabilities which appeared in our derivations. This normalization excludes the possibility of the wave equation and thus eqns (38c′) and (40c′) can be compared with eqn (39c) as shown in Fig. 6. One can see that eqn (38c′) is still the upper bound, but both bounding lines converge at $u_d = 1$. The rather small differences between the three lines indicate the directional persistence $\varpi(u_d)$ to be the key factor affecting the transport parameters.

5. Discussion

We compared the model predictions with the experimental data from Berg & Turner (1990) for wild-type *E. coli* AW405, and interpreted the possible transport mode within capillaries according to our model. Data for smoothly swimming bacteria were not considered here because they did not fit under the protocol of eqn (5) in the bulk phase. Due to the unknown relationship of the angle θ_d with d, we were unable to pinpoint the exact locations of experimental μ_d and V_c as they would appear in Fig. 5. Hence our comparison is only qualitative. Although the current model is based on $\psi = 0$ in the bulk phase, the comparison with the experimental data of *E. coli* ($\psi \simeq 0.3$) is still possible by linearly adjusting the inequality relation (37) for the new bulk value ψ. This adjustment for $\varpi(u_d)$ is shown in Fig. 7 as a generalization to Fig. 5(a) and does not affect the rest of the results in Fig. 5(c)–(d).

Berg & Turner reported the diffusion coefficient (equivalent to our μ_d in this study) to be $(5.19 \pm 1.01) \times 10^{-6}$ cm^2 s^{-1} in capillaries 10 μm in diameter and $(2.63 \pm 0.42) \times 10^{-6}$ cm^2 s^{-1} in capillaries of 50 μm-diam. In view of Fig. 5(c), this trend is consistent with $\varpi(u_d)$ since all

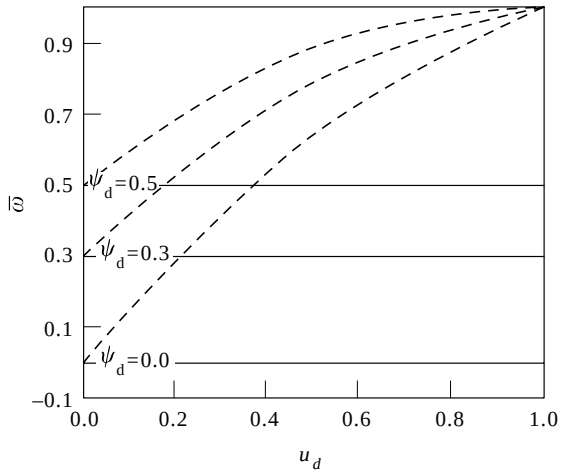

FIG. 7. Generalization of Fig. 5(a) to various bulk values of the directional persistence.

theoretical diffusion coefficients increase as the tube diameter decreases, although we do not learn anything new about $\varpi(u_d)$. Additionally, the empirical function $\theta_d(d)$ is unknown. However, the fact that V_c in 10 μm capillaries is larger than that in 50 μm capillaries indicates that the V_c in capillaries of 10 μm must be located within the diffusive region as shown in Fig. 5(d). Does the directional persistence $\varpi(u_d)$ increase as the tube diameter decreases? If the bacterial transport mode remains diffusional and only the dimensionality changes subject to the tube diameter, both the ratios of the random motility coefficients and chemotactic velocities at two different tube diameters (d_1 and d_2) should be the same as $(1 + u_{d,1} + u_{d,1}^2)/(1 + u_{d,2} + u_{d,2}^2)$ according to eqns (39c, d). The ratio of the μ_d at $d = 10$ and 50 μm, if adopting the above reported values, is $5.2/2.63 = 1.97 \simeq 2.0$; while from Fig. 5 in the paper of Berg & Turner (1990) the ratios of V_c at the above two diameters also are around 2.0 over a wide range of L-aspartate concentrations. From our model, this constant ratio implies that (i) the geometrical constraint is universal and independent of receptor saturation with attractant concentration, (ii) the directional persistence $\varpi(u_d)$ does not increase with u_d but remains at the bulk value even when d is as small as 10 μm. If, however, one adopts the values listed in the last row of Table 3 from Berg & Turner (1990), the ratio for μ_d becomes $6.1/2.6 = 2.34 > 2.0$, indicating a slight increase in $\varpi(u_d)$ in comparison with the bulk phase. The

slight difference stems from experimental errors within tolerable ranges, and therefore a conclusion cannot be reached. All in all, one can at least conclude that $\varpi(u_d)$ appears to increase with the decreases of the tube diameter in a rather mild fashion such that the overall transport mode is still diffusional even in a capillary of 10 μm in diameter. The geometrical effect of a 10 μm capillary only restricts the dimensionality of bacterial motion, characterized by the value of θ_d.

Apparently *E. coli* cannot swim *crosswise* ($\theta_d < \theta < \pi - \theta_d$) but can still swim up or down the capillary of a diameter as small as 10 μm. This explanation is possible according to another study of Berg & Turner (1995) for the swimming orientation of *E. coli*. They concluded that *E. coli* does not possess a chemoreceptor-localized nose (see Parkinson & Blair, 1993) because it swims with equal probability from either end. That is, the cell body does not flip over when it fully reverses the runs. However, the flagellar bundle which acts as the propulsion force still needs to be repositioned behind the cell body when the bacterium reverses swimming directions. The mechanical properties of flagella become increasingly important especially when d decreases below 10 μm. The images of *E. coli* in a capillary of 6 μm (Liu & Papadopoulos, 1995) show significant directional persistence. Although 6 μm is still larger than the typical body size of *E. coli*, it is comparable to the typical flagellar length. Liu & Papadopoulos believed the one-dimensional wave motion should be attributed to flagellar rigidity. It appears that the directional persistence $\varpi(u_d)$ for *E. coli* remains quite a constant bulk value before the tube diameter decreases down to

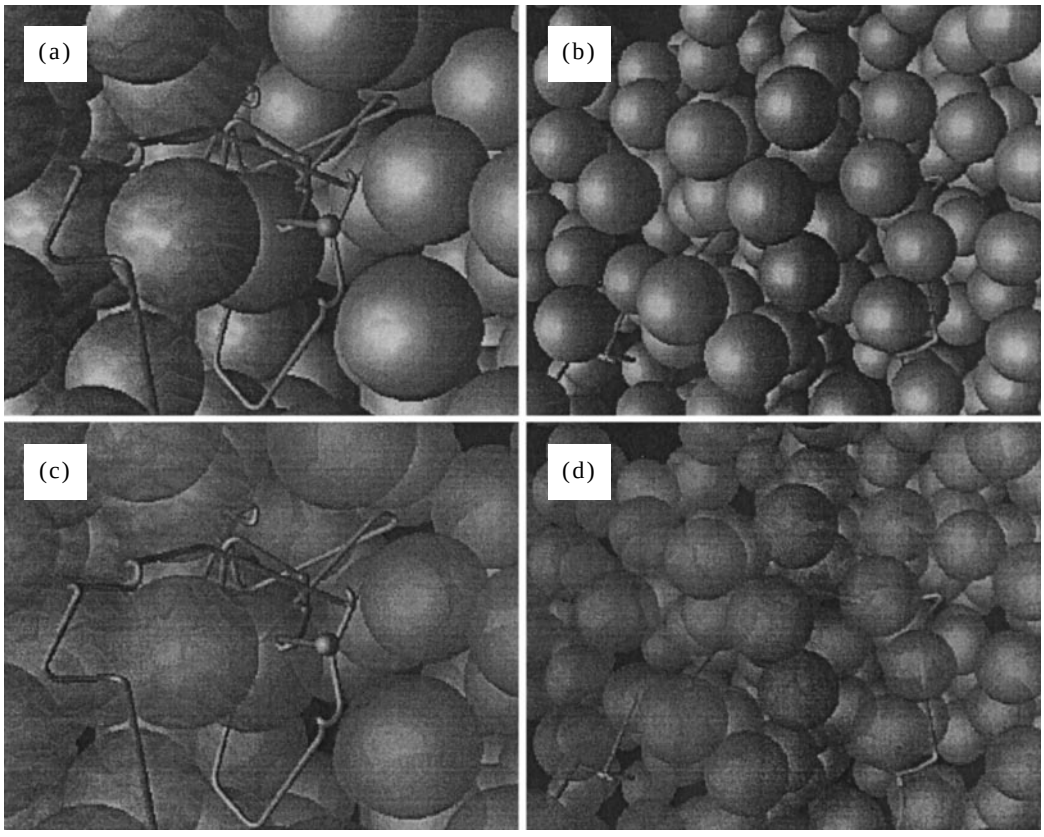

FIG. 8. Monte Carlo simulation of bacterial trajectories with different boundary conditions. Both simulations were executed in the same porous medium composed of non-overlapping, uniform-sized particles for 5 s: (a) adopted diffusive reflection; (b) pseudo-specular reflection as the boundary condition on the particle surface. Some of the solid particles have been removed for visual clarity; (a) was set at an enlarged view due to the smaller mean-squared displacement; (c) and (d) correspond to (a) and (b), respectively, with a reduced opacity (=0.5) for solid spheres so the blocked trajectories can still be observed.

$10\,\mu$m, and then starts rising significantly between $d = 10 \sim 6\,\mu$m as it crosses over the middle line in Fig. 5(a) to the wave region. This sudden rise in $\varpi(u_d)$ results from the geometrical interference associated with the repositioning of the flagellar bundle when d is comparable to the flagellar length.

5.1. SIMULATION IN POROUS MEDIA

Based on the tube guidance exhibited in experiments, we became interested in how a similar guidance may affect bacterial trajectories in a porous medium consisting of randomly packed solid spheres. Suppose the interstitial pores are narrow enough to exert a similar guiding influence upon bacterial motion, but will not halt them with clogging. What will be the impact of this guidance on the macroscopic transport? In Fig. 8 we present two Monte-Carlo simulations of bacterial trajectories within a porous medium. The simulation methodology is similar to Duffy *et al*. (1995) but with an emphasis on the boundary conditions. Figure 8(a) was generated employing diffusive reflection on the particle surface as the boundary condition, which means the rebound angle is independent of the incident angle and is equally probable in all directions. In (b) we adopted a pseudo-specular reflection boundary condition in the sense that the bacterial rebound angle from the particle surface is confined between swimming parallel to the particle surface and the specular reflection angle (see Fig. 9). Hence, although the simulated bacterium still tumbles and turns in free space, it always slides through the interstitial pores whenever approaching the solid particle. This scenario is conceptually equivalent to including a lubricant layer between the solid surface and the bacterium.

With this approach, we had two very different simulation outcomes. In (a) the bacterial trajectories are clearly confined in a local area for a period of time, yielding a smaller mean-squared displacement than in the bulk phase. We obtained in (b) a less curved trajectory produced by the lubricant boundary condition and a larger mean-squared displacement than in the bulk phase, i.e. a larger diffusion coefficient. As a result, the trajectories and running directions also are dominated by the interior structure of

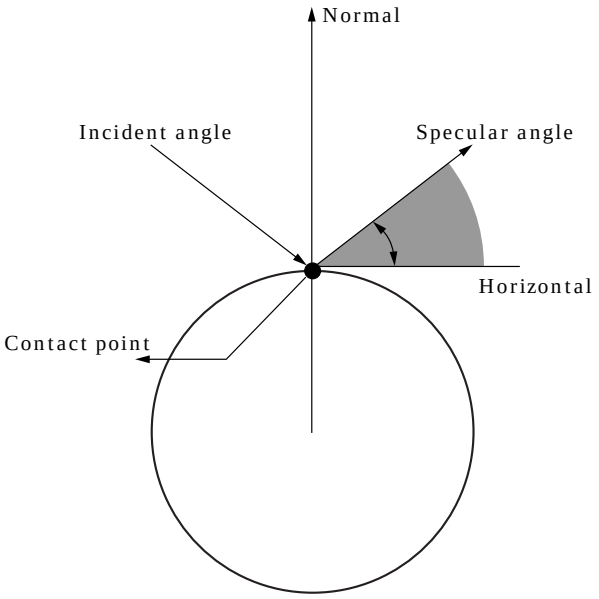

FIG. 9. Boundary condition for pseudo-specular reflection. Bacterial rebound angle after collisions on the particle surface was randomly generated in the shaded area between the horizontal line and the specular angle. The effect of the cellular excluded volume has been included in the particle diameter. The incident and the rebound vectors were assumed to be on the same plane.

porous media and cannot efficiently respond to a spatial chemical gradient (simulation data not shown). Nevertheless, such enhanced bacterial transport in porous media has never been reported (e.g. the experiments of Sharma *et al*., 1993, 1994) mostly because of the dominant adsorption and growth conditions in these experiments. However, in the experiments of Berg & Turner (1990) and Liu & Papadopoulos (1995, 1996, 1997) the bacterial attachment on glass surface had been kept to the minimum extent.

6. Conclusion

In this work we have proposed a phenomenological turning model and incorporated it into the cell balance equation to study the dimensional reduction in random motion and the increase in directional persistence within a long cylindrical tube. Two key factors are the exclusive polar angle θ_d that accounts for the reduction in dimensionality, and the directional persistence ϖ in the tube that controls the transition between a wave equation and a diffusion equation. Both parameters are empiri-

cal functions of the tube diameter, and independent of each other in the sense of eqn (37). As a preliminary step, we have qualitatively verified the bacterial transport mode in tubes of 10 μm-diameter to be diffusional without an obvious increase in directional persistence $\varpi(u_d)$. The increases in μ_d and V_c are due to the reduced dimensionality of random motion due to the constricted geometry.

The concepts presented in this model are not intended to be an endorsement of any particular real transport mechanism, but rather are offered as a means of stimulating further discussion and improvement in our ability to evaluate the rationale of bacterial transport within small tubes. Even though satisfactory agreement between the model predictions and available experimental data indicates our analysis to be capable of predicting possible behaviors and trends, the prediction cannot be complete because of insufficient baseline information. A reasonable agreement between existing experimental results and model predictions does not, of course, demonstrate the validity of the model. It does, however, show that further experiments, probably of a different design, would be required to establish if the model needs to be further modified. Recently a procedure for experimental and data analyses has been proposed by Chen (1997) to quantify the empirical functions $\varpi(d)$ and $u_d(d)$. As a subject demanding more exploration, we also call for more experimental work and theoretical study in order to facilitate further examination of the present state of model assessment. As studies such as these are completed, the initial characterization can be upgraded and refined.

This research is supported by a grant from the IBM Environmental Research Program. However, any opinions, findings, and conclusions or recommendations expressed in this material are those of the authors and do not reflect the view of the IBM Corporation.

REFERENCES

Adler, J. (1966). Chemotaxis in bacteria. *Science* **153,** 708–716.

Alt, W. (1980). Biased random walk models for chemotaxis and related diffusion approximations. *J. Math. Biol.* **9,** 147–177.

Anderson, J. L. (1981). Configurational effect on the reflection coefficient for rigid solutes in capillary pores. *J. theor. Biol.* **90,** 405–426.

Anderson, J. L. & Quinn, J. A. (1974). Restricted transport in small pores. A model for steric exclusion and hindered particle motion. *Biophys. J.* **14,** 130–150.

Barton, J. W. & Ford, R. M. (1995). Determination of effective transport coefficients for bacterial migration in sand columns. *Appl. Environ. Biol.* **61,** 3329–3335.

Barton, J. W. & Ford, R. M. (1997). Mathematical model for characterization of bacterial migration through sand cores. *Biotechnol. Bioeng.* **53,** 487–496.

Berg, H. C. & Brown, D. A. (1972). Chemotaxis in *Escherichia coli* analyzed by three-dimensional tracking. *Nature* **239,** 500–504.

Berg, H. C. & Turner, L. (1990). Chemotaxis of bacteria in glass capillary arrays. *Biophys. J.* **58,** 919–930.

Berg, H. C. & Turner, L. (1995). Cells of *Escherichia coli* swim either end forward. *Proc. Natl. Acad. Sci. U.S.A.* **92,** 477–479.

Biondi, S. A., Quinn, J. A. & Goldfine, H. (1998). Random motility of swimming bacteria in restricted geometries. *AIChE J.* **44,** 1923–1929.

Brenner, H. & Gaydos, L. J. (1977). The constrained Brownian movement of spherical particles in cylindrical pores of comparable radius. *J. Colloid Interface Sci.* **58,** 312–356.

Chen, K. C. (1997). Transport theory of motile bacteria in aqueous phase and small capillaries. Ph.D. Thesis, University of Virginia.

Chen, K. C., Ford, R. M. & Cummings, P. T. (1999). Perturbation expansion of Alt's cell balance equations reduces to Segal's 1-D equations for shallow chemoattractant gradients. *SIAM J. Appl. Math.* **59,** 35–57.

Chen, K. C., Ford, R. M. & Cummings, P. T. (1998). The global turning probability density function for motile bacteria and its applications. *J. theor. Biol.* (in press).

Deen, W. M. (1987). Hindered transport of large molecules in liquid-filled pores. *AIChE J.* **33,** 1409–1425.

Derjaguin, B. V. & Fedyakin, N. N. (1993). Complete specular reflection of molecules at low angles of incidence and its effect on the molecular flow of gases through very narrow capillaries. *Progr. Surf. Sci.* **43,** 290–301.

Duffy, K. J., Ford, R. M. & Cummings, P. T. (1995). Random walk calculations for bacterial migration in porous media. *Biophys. J.* **68,** 800–806.

Ford, R. M. & Cummings, P. T. (1992). On the relationship between cell balance equations for chemotactic cell populations. *SIAM J. Appl. Math.* **52,** 1426–1441.

Ford, R. M., Phillips, B. R., Quinn, J. A. & Lauffenburger, D. A. (1991). Measurement of bacterial random motility and chemotaxis coefficients: I. Stopped-flow diffusion chamber assay. *Biotechnol. Bioeng.* **37,** 647–660.

Froment, G. F. & Bischoff, K. B. (1979). *Chemical Reactor Analysis and Design*. New York: John Wiley & Sons.

Frymier, P. D. & Ford, R. M. (1997). Analysis of bacterial swimming speed approaching a solid–liquid interface. *AIChE J.* **43,** 1341–1347.

Frymier, P. D., Ford, R. M., Berg, H. C. & Cummings, P. T. (1995). Three-dimensional tracking of motile bacteria near a solid planar surface. *Proc. Natl. Acad. Sci. U.S.A.* **92,** 6195–6199.

Happel, J. & Brenner, H. (1983). *Low Reynolds Number Hydrodynamics*. Englewood Cliffs, NJ: Prentice-Hall.

Holz, M. & Chen, S.-H. (1979). Spatio-temporal structure on migrating chemotactic band of *Escherichia coli*. *Biophys. J.* **26,** 243–262.
Keller, E. F. & Segel, L. A. (1971). Models for chemotaxis. *J. theor. Biol.* **30,** 225–234.
Kennard, E. H. (1938). *Kinetics Theory of Gases*. New York: McGraw-Hill.
Knudsen, M. (1909). The laws of molecular flow and of inner friction flow of gases through tubes. *Annal. Phys.* **28,** 75–130.
Krishna, R. & Wesselingh, J. A. (1997). The Maxwell–Stefan approach to mass transfer. *Chem. Eng. Sci.* **52,** 861–911.
Liu, Z. & Papadopoulos, K. D. (1995). Unidirectional motility of *Escherichia coli* in restrictive capillaries. *Appl. Environ. Microbiol.* **61,** 3567–3572.
Liu, Z. & Papadopoulos, K. D. (1996). A method for measuring bacterial chemotaxis parameters in a micro-capillary. *Biotechnol. Bioeng.* **51,** 120–126.
Liu, Z., Chen, W. & Papadopoulos, K. D. (1997). Bacterial motility, collisions, and aggregation in a 3-μm-diameter capillary. *Biotechnol. Bioeng.* **53,** 238–241.
Lovely, P. S. & Dahlquist, F. W. (1975). Statistical measures of bacterial motility and chemotaxis. *J. theor. Biol.* **50,** 477–496.
Macnab, R. M. & Koshland, D. E., Jr. (1972). The gradient-sensing mechanism in bacterial chemotaxis. *Proc. Natl. Acad. Sci. U.S.A.* **69,** 2509–2512.
Mesibov, R., Ordal, G. W. & Adler, J. (1973). The range of attractant concentrations for bacterial chemotaxis and the threshold and size of response over this range. *J. Gen. Physol.* **62,** 203–223.
Othmer, H. G., Dunbar, S. R. & Alt, W. (1988). Models of dispersal in biological systems. *J. Math. Biol.* **26,** 263–298.
Parkinson, J. S. & Blair, D. F. (1993). Does *E. coli* have a nose? *Science* **259,** 1701–1702.
Phillips, B. R. (1992). The random movement of swimming bacteria: II. Simulations of hindered motility in small pore. Ph.D. Thesis, University of Pennsylvania.
Phillips, B. R., Quinn, J. A. & Goldfine, H. (1994). Random motility of swimming bacteria: single cells compared with cell populations. *AIChE J.* **40,** 334–348.
Pollard, W. G. & Present, R. D. (1948). On gaseous self-diffusion in long capillary tubes. *Phys. Rev.* **73,** 762–774.
Ramia, M., Tullock, D. L. & Phan-Thien, N. (1993). The role of hydrodynamic interaction in the locomotion of microorganisms. *Biophys. J.* **65,** 755–778.
Rivero, M. A., Tranquillo, R. T., Buettner, H. M. & Lauffenberger, D. A. (1989). Transport models for chemotactic cell populations based on individual cell behavior. *Chem. Eng. Sci.* **44,** 2881–2897.
Segall, J. E., Block, S. M. & Berg, H. C. (1986). Temporal comparisons in bacterial chemotaxis. *Proc. Natl. Acad. Sci. U.S.A.* **83,** 8987–8991.
Segel, L. A. (1976). Incorporation of receptor kinetics into a model for bacterial chemotaxis. *J. theor. Biol.* **57,** 23–42.
Segel, L. A. (1977). A theoretical study of receptor mechanisms in bacterial chemotaxis. *SIAM J. Appl. Math.* **32,** 653–665.
Sharma, P. J. & McInerney, M. J. (1994). Effect of grain size on bacterial penetration, reproduction, and metabolic activity in porous glass bead chambers. *Appl. Environ. Biol.* **60,** 1481–1486.
Sharma, P. K., McInerney, M. J. & Knapp, R. M. (1993). *In situ* growth and activity and modes of penetration of *Escherichia coli* in unconsolidated porous materials. *Appl. Environ. Biol.* **59,** 3686–3694.
Spudich, J. L. & Koshland, D. E., Jr. (1975). Quantitation of the sensory in bacterial chemotaxis. *Proc. Natl. Acad. Sci. U.S.A.* **72,** 710–713.
Wang, P. C. & Chen, S.-H. (1986). Quasi-elastic light scattering from migrating chemotactic bands of *Escherichia coli*. *Biophys. J.* **49,** 1205–1214.

APPENDIX

List of Symbols

a: attractant concentration
d: tube diameter
$\hat{\mathbf{e}}_x$, $\hat{\mathbf{e}}_y$, $\hat{\mathbf{e}}_z$: principle axes of x, y and z
f: sticking coefficient
h, g: constant turning probability density function in P-regions, defined in eqn (26)
n: bacterial angular number density
n^+, n^-: bacterial subpopulation densities, defined in eqns (16a, b)
c: bacterial bulk density ($=n^+ + n^-$), defined below eqns (16)
$\mathbf{r}$: position vector
$\hat{\mathbf{s}}$: unit swimming direction vector before tumbling
$\hat{\mathbf{s}}'$: unit swimming direction vector after tumbling
t: time
t_0: initial time when chemical gradients are imposed
$p_{r,t}$: one-dimensional reversal probability subject to tumbling, eqn (18)
$p_{r,c}$: one-dimensional reversal probability subject to wall collisions, eqn (24)
p_t: bacterial tumbling frequency
p_1: bacterial isotropic tumbling frequency
u_d $\cos\theta_d$
v: bacterial three-dimensional swimming speed
z: the tube axis
E: long-range interaction potential distribution in the radial direction, eqn (14)
J: one-dimensional bacterial flux along z, defined in eqn (19)

K: global reduced angular turning probability density function, defined in eqn (10)

N: bacterial angular number density integrated over cross section of tubes, defined in eqn (8)

N_b: number of bacterial receptors bound with attractant molecules

Q: bacterial metabolic capacity, eqn (14)

Kn: Knudsen number, ratio of mean run length to tube diameter λ/d

V_c: chemotactic velocity

Greek letters

η: radial axis

κ: angular mean run length

λ: bacterial mean run length

μ^o: diffusion coefficient of bacterial populations in bulk phase, defined in eqn (1)

μ^k diffusion coefficient of bacterial populations in a tube predicted by Knudsen equation, eqn (3)

μ_d: diffusion coefficient of bacterial populations in a tube of diameter d, eqn (4)

ν: sensitivity factor between chemotactic responses (anisotropic p_t) and chemical gradients, defined below eqn (22)

ψ: directional persistence in bulk phase, defined in eqn (25b)

θ: polar angle of bacterial running vector relative to z

θ_d: polar angle of the turning gap in the global turning PDF, see Fig. 4

ϕ: azimuthal angle of bacterial running vector relative to z, in spherical coordinates

φ: azimuthal angle of cylindrical tubes, in cylindrical coordinates

$\mathbf{\Omega}_=$: bacterial orientation function in P-regions

$\mathbf{\Omega}_\perp$: bacterial orientation function in N-region

Υ: global reduced scattering probability density function, appeared in eqn (15)

ϖ: directional persistence in a tube of diameter d, defined in eqn (25b′)

ς_f, ς_b: forward and backward mean turning probability densities, defined in eqns (27)

ξ: strength of one-dimensional attractant gradients, defined below eqn (22)